NASA CR-120944
GDCA-DDB72-003

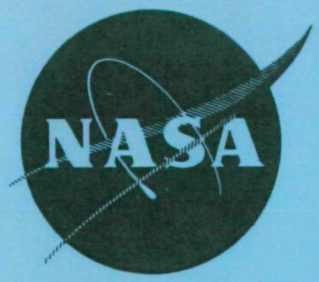

AN ANALYTICAL STUDY OF REDUCED-GRAVITY LIQUID REORIENTATION USING A SIMPLIFIED MARKER AND CELL TECHNIQUE

by
W.S. Betts, Jr.

prepared for
NATIONAL AERONAUTICS AND SPACE ADMINISTRATION
NASA Lewis Research Center
Contract NAS 3-14361

GENERAL DYNAMICS
Convair Aerospace Division

NASA CR-120944
GDCA-DDB72-003

AN ANALYTICAL STUDY OF REDUCED-GRAVITY LIQUID REORIENTATION USING A SIMPLIFIED MARKER AND CELL TECHNIQUE

by W. S. Betts, Jr.

Convair Aerospace Division of General Dynamics
San Diego, California

prepared for

NATIONAL AERONAUTICS AND SPACE ADMINISTRATION

NASA Lewis Research Center
Contract NAS3-14361

1. Report No.	2. Government Accession No.	3. Recipient's Catalog No.
NASA CR-120944		

4. Title and Subtitle	5. Report Date
An Analytical Study of Reduced-Gravity Liquid Reorientation Using a Simplified Marker and Cell Technique	August 1972
	6. Performing Organization Code
7. Author(s)	8. Performing Organization Report No.
W. S. Betts, Jr.	GDCA-DDB72-003
	10. Work Unit No.
9. Performing Organization Name and Address	
Convair Aerospace Division of General Dynamics San Diego, California 92112	11. Contract or Grant No. NAS3-14361
	13. Type of Report and Period Covered Contract Report
12. Sponsoring Agency Name and Address	
National Aeronautics and Space Administration Washington, D.C. 20546	14. Sponsoring Agency Code

15. Supplementary Notes

Project Manager, William J. Masica, Chemical Propulsion Division
NASA Lewis Research Center, Cleveland, Ohio

16. Abstract

A computer program called HOPI was developed to predict reorientation flow dynamics, wherein liquid moves from one end of a closed, partially filled, rigid container to the other end under the influence of container acceleration. Tne program uses the Simplified Marker and Cell (SMAC) numerical technique and, using explicit finite-differencing, solves the Navier-Stokes equations for an incompressible viscous fluid. The effects of turbulence are also simulated in the program. HOPI can consider curved as well as straight walled boundaries. Both free-surface and confined flows can be calculated. The program was used to simulate five liquid reorientation cases. Three of these cases simulated actual NASA LeRC drop tower test conditions while two cases simulated full-scale Centaur tank conditions.

It was concluded that while HOPI can be used to analytically determine the fluid motion in a typical settling problem, there is a current need to optimize HOPI. This includes both reducing the computer usage time and also reducing the core storage required for a given size problem.

17. Key Words (Suggested by Author(s))	18. Distribution Statement
Liquid Reorientation, Incompressible Fluid Mechanics Flow, Marker and Cell	Unclassificed - Unlimited

19. Security Classif. (of this report)	20. Security Classif. (of this page)	21. No. of Pages	22. Price*
Unclassified	Unclassified	85	

* For sale by the National Technical Information Service, Springfield, Virginia 22151

FOREWORD

The research described herein, which was conducted by the Convair Aerospace Division, was performed under NASA Contract NAS3-14361. The work was done under the management of the NASA Project Manager, Mr. William J. Masica, NASA-Lewis Research Center. The study was completed under the direction of Convair project leader, Mr. W. S. Betts. The author wishes to acknowledge the direction of Mr. Masica, the efforts of Mr. K. R. Burton (project leader February 1971 to August 1971) and the assistance received from Mr. J. A. Viecelli of Lawrence Radiation Laboratory.

ABSTRACT

A computer program called HOPI was developed to predict reorientation flow dynamics, wherein liquid moves from one end of a closed, partially filled, rigid container to the other end under the influence of container acceleration. The program uses the Simplified Marker and Cell (SMAC) numerical technique and, using explicit finite-differencing, solves the Navier-Stokes equations for an incompressible viscous fluid. The effects of turbulence are also simulated in the program. HOPI can consider curved as well as straight walled boundaries. Both free-surface and confined flows can be calculated. The program was used to simulate five liquid reorientation cases. Three of these cases simulated actual NASA LeRC drop tower test conditions while two cases simulated full-scale Centaur tank conditions.

It was concluded that while HOPI can be used to analytically determine the fluid motion in a typical settling problem, there is a current need to optimize HOPI. This includes both reducing the computer usage time and also reducing the core storage required for a given size problem.

TABLE OF CONTENTS

LIST OF FIGURES

LIST OF FIGURES, Contd

SUMMARY

This report covers the work performed under NASA/LeRC Contract NAS3-14361 by the Convair Aerospace division of General Dynamics during the period from February 1971 thru April 1972.

The objective of this contract was the development of a numerical method to predict reorientation or settling flow dynamics, wherein liquid moves from one end of a closed, partially filled, rigid container to the other end under the influence of container acceleration.

Convair used the Navier-Stokes and the continuity equations for incompressible, viscous fluid as the basic equations governing the reorientation flow dynamics. The equations were programmed using explicit finite differencing for two-dimensional planer and three-dimensional axisymmetric problems. The Simplified Marker and Cell (SMAC) numerical technique was used to determine liquid-vapor interface positions.

Convair uses a turbulent kinematic viscosity relationship to analytically approximate the effects of turbulence

$$\nu_{turb} = \text{TURB} \times \ell^2 \max\left(\left|\frac{\partial v}{\partial r}\right|, \left|\frac{\partial u}{\partial z}\right|\right)$$

where TURB is an empirical factor which is used to correlate the data. A value of 0.05 was found to best correlate the LeRC drop tower results.

$$\ell = \begin{cases} \text{DR if } \left|\frac{\partial v}{\partial r}\right| > \left|\frac{\partial u}{\partial z}\right| \\ \text{DZ if } \left|\frac{\partial u}{\partial z}\right| > \left|\frac{\partial v}{\partial r}\right| \end{cases}$$

where DR and DZ are the grid dimensions and u and v are the velocity components in the radial (r) and axial (z) directions, respectively.

The viscosity of a fluid was treated as the sum of the molecular viscosity and turbulent viscosity. For the reorientation flow cases run during the contract the magnitude of the turbulent viscosity was generally at least an order of magnitude greater than the molecular viscosity.

Convair developed a computer code called HOPI using the equations formulated in the analytical studies. It is noted that while HOPI is restricted to two dimensional

problems the basic SMAC technique may be three dimensional. HOPI can handle curved as well as straight-walled boundaries. It has the ability to calculate both free-surface and confined flows. It can be used in either cylindrical or plane geometry. The size of the computing mesh is easily changed from problem to problem. The grid dimension in each direction must be constant through the grid mesh, although the grid dimensions in the radial and axial direction may differ. Gravitational effects may be included in any orientation however it is noted that HOPI can only compute axisymmetric flow when a cylindrical geometry is used. For any given time interval the gravitational acceleration must be constant. HOPI has a surface pressure interpolation scheme that prevents unrealistic breakup of the surface.

Convair used the computer program HOPI to simulate five liquid reorientation cases. Three of the cases simulated actual NASA LeRC drop tower test conditions and were used to provide confidence in the results generated by HOPI. The additional two cases simulated full-scale Centaur tank conditions. The cylindrical tanks had height to diameter ratio of two, hemispherical forward and spherical segment bottom dome, with a radius of 7 cm for drop tower cases and 150 cm for full scale cases. In all cases the initial interface shape corresponded to a Bond number of 10. The reorientation Bond numbers ranged from 100 to 450.

The experience gained in running these cases indicates that HOPI can be used to analytically determine the fluid motion in a cryogen storage tank under a continuous settling load. However, there is a current need to optimize HOPI. This includes reducing the computer usage time and also reducing the core usage required for a given size problem. To reduce the computer usage time it is recommended that HOPI be modified to handle variable grid mesh and to change the subscripting from double to single throughout the code. To reduce the core storage it is recommended that overlaying be used.

1.0 INTRODUCTION

Auxiliary thrustors are used to create reduced-gravity environments to control and locate liquid surfaces in space vehicle systems. The continual use of even small thrustors for long-term missions can result in undesirable weight penalties and, thus, their operation may have to be intermittent. During the off-times, the liquid surface may be destabilized and relocated due to disturbances acting on the vehicle. Various passive retention devices such as capillary baffles might be used to control the location of the liquid, but it appears that, at least for large cryogenic propellant systems, reduced-gravity auxiliary thrustors will remain a primary method of control. The auxiliary thrustors will be relied upon to settle or reorient the propellant back to its desired location prior to restart or venting operations. The thrust and time required to settle efficiently and reliably are vital design factors. The initial destabilization and ensuing flow dynamics have been studied analytically, but reorientation time estimates are still derived almost entirely from empirical results based on scale-model experiments. References 1 through 7 discuss aspects of this reorientation problem.

During this contract, a computer program called HOPI was developed which can be used to predict reorientation flow dynamics, wherein liquid moves from one end of a closed partially filled, rigid container to the other end under the influence of container acceleration. This computer program numerically solves the Navier-Stokes equations for viscous incompressible fluids using the Simplified Marker-and-Cell (SMAC) technique. The basic development of this technique is given in Reference 8. One limitation of the program described in Reference 8 is that it cannot consider curved boundaries. Basic techniques to handle curved boundaries were developed by Viecelli in Reference 9.

The objective of this study is to extend the scope of past analytic studies of reorientation to the liquid-liquid impingement phase and to calculate during this phase interface profiles and liquid volume collection rates. The region of particular interest is reorientation Bond numbers of 100 to 500. Representative cases were calculated to compare directly with drop tower experiments and to corroborate empirical results for full-scale vehicle propellant tank configurations.

2.0 DISCUSSION

In the Simplified MAC (SMAC) technique, the procedure for a calculational cycle is as follows:

1. A tentative field of advanced-time velocities is calculated by using an arbitrary pressure field within the field, but with a pressure boundary condition at the free surface satisfying the normal stress condition. Correct velocity boundary conditions assure that this tentative velocity field contains the correct vorticity at every interior point in the field. The tentative velocities do not satisfy continuity (i.e., $\nabla \cdot V = 0$).

2. The tentative velocities are modified to their final values so as to preserve the vorticity at every point. A potential function is employed, determined by the requirement that it convert the velocity field to one which satisfies the incompressibility condition everywhere.

The computer program developed during this contract is called HOPI, Reference 10. It handles two-dimensional or axisymmetric three-dimensional problems involving incompressible Newtonian fluids. In the following sections the basic equations and techniques used in HOPI are presented.

2.1 EQUATIONS USED IN HOPI

The basic differential equations are

$$\frac{\partial u}{\partial t} + \frac{1}{r^\alpha}\frac{\partial r^\alpha u^2}{\partial r} + \frac{\partial uv}{\partial z} = -\frac{\partial \phi}{\partial r} + g_r + \nu \frac{\partial}{\partial z}\left(\frac{\partial u}{\partial z} - \frac{\partial v}{\partial r}\right),$$

$$\frac{\partial v}{\partial t} + \frac{1}{r^\alpha}\frac{\partial r^\alpha uv}{\partial r} + \frac{\partial v^2}{\partial z} = -\frac{\partial \phi}{\partial z} + g_z - \frac{\nu}{r^\alpha}\frac{\partial}{\partial r}\left[r^\alpha\left(\frac{\partial u}{\partial z} - \frac{\partial v}{\partial r}\right)\right],$$

and

$$D = \frac{1}{r^\alpha}\frac{\partial r^\alpha u}{\partial r} + \frac{\partial v}{\partial z} = 0$$

The velocity components, u and v, are respectively in the r and z directions, and the pressure, ϕ, is normalized to unity density. The two components of gravitational

acceleration are g_r and g_z as indicated below. Plane (Cartesian) coordinates have $\alpha = 0$, and in cylindrical coordinates, $\alpha = 1.0$.

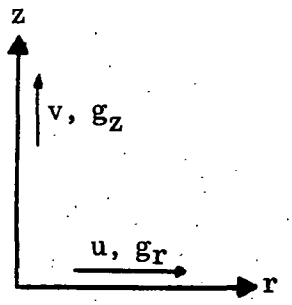

In differential form, the equation for transport of vorticity, ω, is independent of the pressure, so that any field of pressure inserted into the Navier-Stokes equations will assure that the resulting velocity field carries the correct vorticity. An arbitrary pressure field will not, however, assure the vanishing of D, but if the velocity field is altered by the addition of the gradient of an appropriate potential function, the resulting field will carry the same vorticity, have vanishing D, and accordingly will be uniquely determined, hence correct.

This is the essence of the procedure for the finite difference solutions. As a starting point, the equations are written in the following form.

$$\frac{\tilde{u}^{n+1}_{i+1/2,j} - u^{n}_{i+1/2,j}}{\delta t} =$$

$$\frac{r^{\alpha}_{i} u^{n}_{i+1/2,j} \; u^{n}_{i-1/2,j} - r^{\alpha}_{i+1} \; u^{n}_{i+3/2,j} \; u^{n}_{i+1/2,j}}{r^{\alpha}_{i+1/2} \, \delta r}$$

$$+ \frac{u^{n}_{i+1/2,j-1/2} \; v^{n}_{i+1/2,j-1/2} - u^{n}_{i+1/2,\,j+1/2} \; v^{n}_{i+1/2,\,j+1/2}}{\delta z}$$

$$+ \frac{\psi_{i,j} - \psi_{i+1,j}}{\delta r} + g_r$$

$$+ \nu \left[\frac{1}{\delta z^2} \left(u^{n}_{i+1/2,j+1} + u^{n}_{i+1/2,j-1} - 2u^{n}_{i+1/2,j} \right) \right.$$

$$\left. - \frac{1}{\delta r \, \delta z} \left(v^{n}_{i+1,j+1/2} - v^{n}_{i+1,j-1/2} - v^{n}_{i,j+1/2} + v^{n}_{i,j-1/2} \right) \right] \qquad (1)$$

$$\frac{\tilde{v}^{n}_{i,j+1/2} - v^{n}_{i,j+1/2}}{\delta t} =$$

$$\frac{r^{\alpha}_{i-1/2}\, u^{n}_{i-1/2,j+1/2}\, v^{n}_{i-1/2,j+1/2} - r^{\alpha}_{i+1/2}\, u^{n}_{i+1/2,j+1/2}\, v^{n}_{i+1/2,j+1/2}}{r^{\alpha}_{i}\,\delta r}$$

$$+ \frac{v^{n}_{i,j+1/2}\, v^{n}_{i,j-1/2} - v^{n}_{i,j+3/2}\, v^{n}_{i,j+1/2}}{\delta z}$$

$$+ \frac{\psi_{i,j} - \psi_{i,j+1}}{\delta z} + g_z$$

$$- \frac{\nu}{r^{\alpha}_{i}\delta r}\left[r^{\alpha}_{i+1/2}\left(\frac{u^{n}_{i+1/2,j+1} - u^{n}_{i+1/2,j}}{\delta z} \right.\right.$$

$$\left. - \frac{v^{n}_{i+1,j+1/2} - v^{n}_{i,j+1/2}}{\delta r} \right)$$

$$\left. - r^{\alpha}_{i-1/2}\left(\frac{u^{n}_{i-1/2,j+1} - u^{n}_{i-1/2,j}}{\delta z} - \frac{v^{n}_{i,j+1/2} - v^{n}_{i-1,j+1/2}}{\delta r} \right)\right] \qquad (2)$$

and

$$D^{n+1}_{i,j} = \frac{r^{\alpha}_{i+1/2}\, u^{n+1}_{i+1/2,j} - r^{\alpha}_{i-1/2}\, u^{n+1}_{i-1/2,j}}{r^{\alpha}_{i}\,\delta r}$$

$$+ \frac{v^{n+1}_{i,j+1/2} - v^{n+1}_{i,j-1/2}}{\delta z} = 0 \qquad (3)$$

The subscripts refer to position in the finite-difference mesh (see Fig. 1), and the superscript n counts time cycles. The true pressure, ϕ, has been replaced by the arbitrary field, ψ, and accordingly the new-time velocities are marked with tildes.

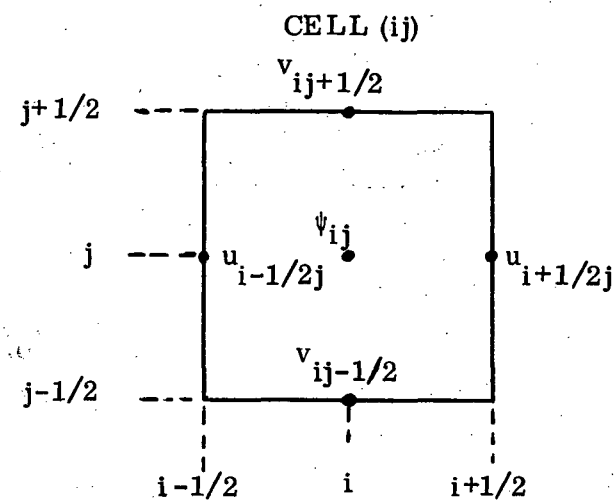

Figure 1. The Location of the Cell Variables in a SMAC Cell

The finite difference equations have been written with explicit (retarded-time) fluxes. Cell-centered momentum convection terms have been written in the ZIP form, which, although continuing to assure internal momentum conservation as in MAC, allows SMAC to conserve momentum in the immediate vicinity of a rigid wall. This type of differencing introduces the definition

$$(u_{i,j})^2 \equiv u_{i-1/2,j}\, u_{i+1/2,j} \tag{4}$$

An advantage of its usage is the removal of a destabilizing truncation error term that occurs in the original form of MAC, (Reference 11).

A finite-difference approximation to the vorticity is

$$\omega^n_{i+1/2,\, j+1/2} \equiv \frac{u^n_{i+1/2,\, j+1} - u^n_{i+1/2,j}}{\delta z} - \frac{v^n_{i+1,j+1/2} - v^n_{i,j+1/2}}{\delta r} \tag{5}$$

with centering at cell corners. Equations (1) and (2) can be combined to obtain a transport expression for $\omega_{i+1/2, j+1/2,}$ which, like the differential equation, is independent of the ψ field. Accordingly, the explicit calculations of the tilde velocities assures that the vorticity at every internal mesh corner point is correct, independent of the choice of ψ. This is not true, however, for corner points that lie on rigid walls, which are not correct until the tilde velocities have been corrected to assure the vanishing of D. For purely explicit calculations, which are acceptable for Reynolds numbers greater than about unity, SMAC vorticity diffusion from the wall is nevertheless correct, because the tilde velocities are based entirely upon the final velocities from the previous cycle, which do agree with the proper wall vorticity.

A cell is flagged as a surface (SUR) cell when it contains fluid, marker particles and it has at least one adjacent neighboring cell which is flagged empty. Marker particles do not perform any function in HOPI calculations other than to indicate the position of any free surface that may be present. On free surfaces the tangential stress condition is

$$\frac{\partial u}{\partial z} + \frac{\partial v}{\partial r} = 0$$

so that $u_{i+1/2, j+1}$ is determined by the equation

$$u_{i+1/2, j+1} = u_{i+1/2, j} - \frac{\delta z}{\delta r} \left(v_{i+1, j+1/2} - v_{i, j+1/2}\right). \tag{6}$$

This assures that the tangential viscous momentum flux vanishes when calculated by Equation (1) for $u_{i+1/2, j}$.

In addition, the normal stress condition is

$$\phi_{i, j} = \phi_{i, j} \text{ (applied)} + \frac{2\nu}{\delta z} \left(v_{i, j+1/2} - v_{i, j-1/2}\right) \tag{7}$$

The applied part of the pressure is specified according to the requirement of the problem while the viscous part assures that there is otherwise no net flux of normal momentum through the surface. It is important that the normal stress condition be placed on the free surface rather than at the center of the surface cell.

The viscosity coefficient υ used in Equations 1 and 2 is the sum of the kinematic molecular viscosity and the turbulent viscosity.

$$\upsilon = \upsilon_{\text{molecular}} + \upsilon_{\text{turb}}$$

The molecular viscosity is an input quantity and is a fluid property. The turbulent viscosity coefficient is calculated internally in the program as indicated below.

$$\upsilon_{\text{turb}} = \text{TURB} \times \ell^2 \max \left(\left| \frac{\partial v}{\partial r} \right|, \left| \frac{\partial u}{\partial z} \right| \right)$$

where

$$\ell = \begin{cases} \text{DR if } \left| \frac{\partial v}{\partial r} \right| > \left| \frac{\partial u}{\partial z} \right| \\ \text{DZ if } \left| \frac{\partial u}{\partial z} \right| > \left| \frac{\partial v}{\partial r} \right| \end{cases}$$

and TURB is an input quantity.

This expression for turbulent viscosity is of the form predicted by both Prandtl's mixing-length theory and Taylor's vorticity transport theory. While other expressions for predicting the turbulent viscosity do exist, the above was selected due to its wide acceptance and simplicity.

Basically a turbulent viscosity is calculated in a cell containing fluid when at least two of its adjacent neighboring cells also contain fluid. The criteria of requiring fluid in adjacent fluid cells is needed so that $\partial v/\partial r$ and $\partial u/\partial z$ can be calculated.

For the reorientation flow cases run during this contract (Section 3) the magnitude of the local turbulent viscosity coefficient was at least an order of magnitude greater than the molecular viscosity coefficient for most of the duration of the problem. This indicates that the viscosity coefficient used in Equations 1 and 2 is mainly a result of the turbulent viscosity coefficient.

2.2 HOPI COMPUTER PROGRAM

This section describes in detail the SMAC calculational cycle in the framework of HOPI. HOPI embodies a number of features that make it a useful tool. Among these are

1. It is written in FORTRAN IV for the CDC-6400 computer.

2. It has the ability to calculate both free-surface and confined flows.

3. It has the ability to calculate either in cylindrical or plane geometry.

4. The size of the computing mesh is easily changed from problem to problem.

5. It has a simple, straightforward setup, allowing different initial conditions and particle resolution in different regions of the mesh.

6. Various boundary conditions are available, along with an obstacle.

7. Gravitational effects may be included in any orientation. However, it is noted that HOPI can only compute axisymmetric flow when a cylindrical geometry is used.

8. Both curved and straight wall boundaries can be used.

The underlying HOPI scheme is now discussed in detail.

2.2.1 COMPUTING MESH. The HOPI computing mesh will handle either cylindrical or plane geometry calculations. The equations are all presented in cylindrical form, however, it is shown in Section 2.2.6 that it is simple to transform them to plane form. The computing mesh as used in cylindrical coordinates (Figure 2) is an infinitely thin radial radial slice from a cylinder. The computing cells become "toroids" of revolution about this cylinder, and are of uniform size in HOPI.

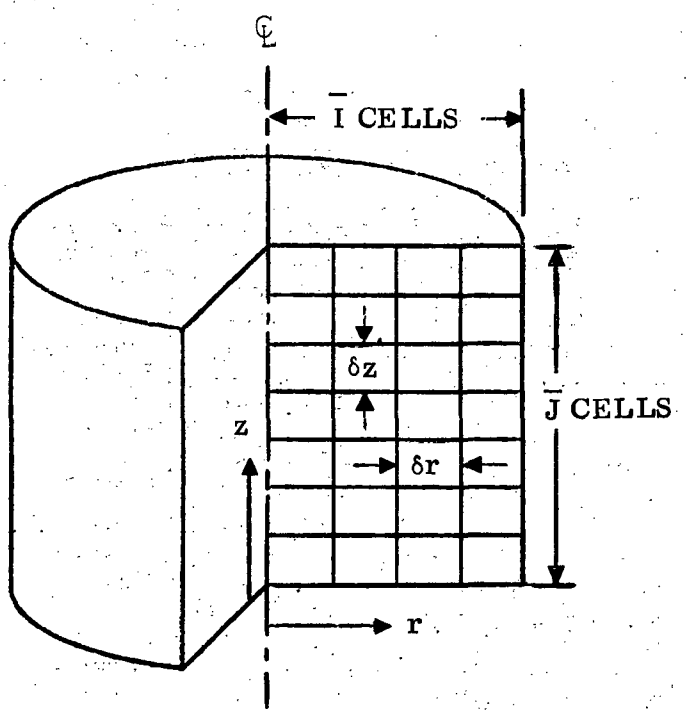

Figure 2. Computing Mesh in Cylindrical Coordinates

The radial coordinate is denoted by r, and the radial cell size is denoted by δr, whereas the axial coordinate is denoted by z, with δz the cell size in the axial direction. The origin is located at the lower left corner of the mesh of cells, the centers of which are labeled with the indices i and j. These indices increase in the r and z directions, respectively. The mesh of cells is $\bar{I}$ (IBAR) cells wide and $\bar{J}$ (JBAR) cells high.

2.2.2 CELL VARIABLES. The primary cell variables are the two components of velocity, u and v, the pseudo-pressure Ψ, and the velocity divergence, D. The centering of these variables about a SMAC cell is shown in Figure 1, where it is seen that the velocities in the radial direction are centered at the left and right edges of the cell, and axial velocities at the top and bottom edges. D, and Ψ are defined at the cell center. In the equations, velocities appear that are not positioned at the cell edges. In these instances, simple averages are calculated. For example

$$(uv)_{i+1/2,\,j-1/2} = \left(\frac{u_{i+1/2,\,j} + u_{i+1/2,\,j-1}}{2}\right)\left(\frac{v_{i,\,j-1/2} + v_{i+1,\,j-1/2}}{2}\right)$$

2.2.3 BASIC TYPES OF CELLS AND THE INDEXING SCHEME. The basic types of cells which may exist within the mesh are described in Figure 3. Use of these flags is demonstrated in Figures 4 and 6.

ARB An OB cell which has a fluid particle within $\epsilon \cdot DR$ of the arbitrary boundary, where ϵ is the boundary sensing parameter and is usually set equal to .25.

BOT A COR cell containing a segment of an arbitrary boundary which has its midpoint and angle being stored in the OB cell just below it.

COR A cell which has a line segment of the arbitrary boundary passing through it, however fluid area to total cell area fraction is less than .25. The fluid area is to the left of the line segment. Also, any cell just outside an OB cell is a COR cell.

EMP The cell is empty (contains no fluid particles).

EOC A cell which is either EMP or COR.

EXT Any cell outside a COR cell.

FUL A cell which contains fluid and has empty neighbor.

LEF A COR cell containing a segment of an arbitrary boundary which has its midpoint and angle being stored in the OB cell just to the left of it.

OB A cell which has a line segment of the arbitrary boundary associated with it (see COR).

OK An ARB cell that does not contain the intersection of a free surface and the boundary.

RIG A COR cell containing a segment of an arbitrary boundary which has its midpoint and angle being stored in the OB cell just to the right of it.

SNC A cell which is also flagged as FUL or SUR and not COR.

SUR A cell which contains fluid and has at least one empty neighbor.

TOP A COR cell containing a segment of an arbitrary boundary which has its midpoint and angle being stored in the OB cell just above it.

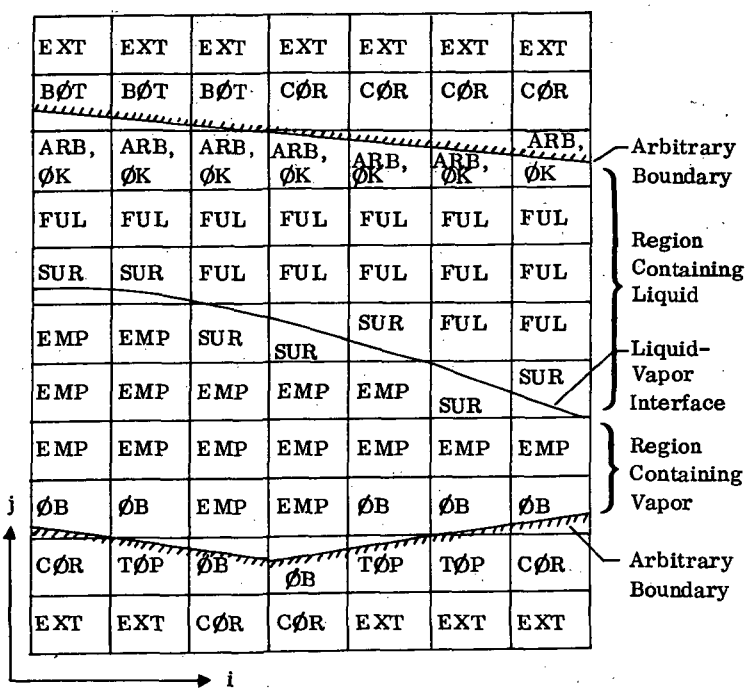

NOTE:
1. All ARB cells are also flagged as ØB.
2. All TØP, BØT, RIG and LEF cells are also flagged as CØR cells.
3. All the above SUR and FUL cells are also flagged SNC.

Figure 3. Grid Network With Typical Cell Flags

In Eulerian programs of the MAC-SMAC type, experience has shown that it is helpful to surround the above-described mesh with a belt of cells lying outside the boundaries. Cells in this belt are called boundary (BND) cells, and they simplify the task of handling boundary conditions, particularly those relating to velocities.

In the FORTRAN code HOPI involving the SMAC equations, we reference "$\psi_{i,j}$" simply as "PSI (I, J)." But "$u_{i+1/2,j}$" cannot be referenced by a "half-integer" index in FORTRAN, so the convention has evolved that "U(I, J)" refers to this velocity, "V(I, J)" in the code actually refers to $v_{i,j+1/2}$.

Given this referencing scheme, the reason becomes apparent for creating a column of BND cells on the left for storing the u's (normal velocities) for the left boundary, and a row of BND cells along the bottom for storing the v's (normal velocities) pertaining to the bottom boundary. In addition, tangential velocities are logically arranged in BND cells on all four sides; their values are based on neighboring u's and v's lying inside, modified through the existing wall boundary condition. With appropriate "outside" velocities thus distributed over the BND cells, the computer code can solve the SMAC equations over the interior cells, picking up velocities on all sides as needed, without having to test for adjacency of a mesh boundary. Variables in BND cells must, however, be updated as the corresponding variables inside change in value.

It is clear that it is possible for a cell to contain a number of flags. For example, a cell could be OB, ARB, FUL, OK, and SNC all at once. In HOPI an NBIT function is used to determine if a flag is set for a given cell. To speed up the computation time certain cell flags such as EOC and SNC were developed, which represent two or more flags. To further speed up the computation time "G" flags were developed as indicated below:

G = 2 implies a COR cell

G = 3 implies an OK cell

G = 4 implies EMP and not COR or EXT cell

G = 5 implies a BND cell

An optimization study indicated that each computation of the form

```
IF (NBIT (10, F(N)) . EQ. 1) GO TO 100
```

takes .386/10,000 seconds while a computation of the form

IF (G(N) . EQ . 1) GO TO 100

takes .141/10,000 seconds.

This shows that it is 2.75 times faster if a G cell flag is used instead of the NBIT function. A given cell can contain only one G flag.

2.2.4 MARKER PARTICLES. In addition to the mesh of Eulerian cells, SMAC employs a set of massless marker particles, which are helpful for allowing a visual representation of the fluid, but whose essential purpose is to define the position of the free surface so that the configuration of SUR cells can be sensed. Beyond this, the marker particles do not enter into the calculation, but are merely embedded in the fluid and are carried along by it. Each cycle the marker particles are moved with a weighted average of the four nearest u's and of the four nearest v's.

2.2.5 BOUNDARY CONDITIONS. In HOPI both straight line and curved wall boundaries can be used. A curved wall is approximated by a series of straight line segments within the grid mesh, where each cell that has part of the curved boundary passing through it contains a straight line segment. Each line segment is formed by joining the two points formed where the curved boundary crossed the rectilinear Eulerian boundary of the cell.

Straight Wall Adjacent to a BND Cell

With reference to Figure 4, the indices i, j refer to the cell inside the system, and i-1, j refer to the BND cell lying just outside.

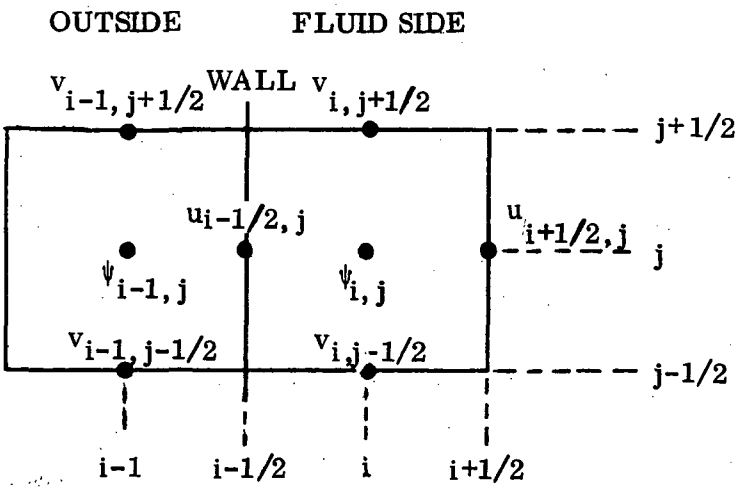

Figure 4. Variable Positions at a SMAC Left Wall

1. FREESLIP: A freeslip boundary represents an axial centerline or a plane of symmetry or a non-adhering surface that exerts no drag upon the fluid. The normal velocity component vanishes at the wall, and there is no gradient in either tangential velocity or in the potential function ψ

$$\begin{cases} u_{i-1/2,j} = 0 \\ v_{i-1,j+1/2} = v_{i,j+1/2}, \\ v_{i-1,j-1/2} = v_{i,j-1/2} \\ \psi_{i-1,j} = \psi_{i,j} \end{cases}$$

2. NOSLIP; A noslip boundary represents a viscous boundary that exerts a drag upon the fluid. This is accomplished by forcing the tangential velocity to go to zero at the wall

$$\begin{cases} u_{i-1/2,j} = 0 \ , \\ v_{i-1,j+1/2} = -v_{i,j+1/2} \ , \\ v_{i-1,j-1/2} = -v_{i,j-1/2} \ , \\ \psi_{i-1,j} = \psi_{i,j} \ . \end{cases}$$

The no slip option is not available for curved wall boundaries. Also, it is noted that often more accurate results might be obtained by imposing the free slip condition on a boundary even when in reality a no slip condition exists. This is true when the grid mesh is too coarse to accurately resolve the detailed motion of the boundary layer resulting from a no slip condition. This was true during the cases run during this contract. Therefore, for the cases reported in this report the free slip boundary condition was always imposed on every boundary.

Curved Wall Boundaries

The basic technique for handling curved-wall boundaries was developed by Viecelli in Reference 9. Only the case of free-slip boundary conditions exist for curved-wall boundaries. The motion of an interface between a liquid and a curved wall is equivalent to that of a free surface with an applied pressure distribution. Given any interfacial shape or motion one can produce that same shape or motion with some unique pressure distribution applied to a free surface. This is the basis for arbitrary boundary calculations.

A curved wall is specified by a locus of points. These points might be the edge intersection points of a mesh covering the wall or body; however, in general the points will not lie on any of the Eulerian mesh lines used in the finite difference solution of the hydrodynamic equations. The first step is to connect successive points with straight lines and find all of the intersections of these segments with the underlying Eulerian mesh. One can then represent the boundary section lying inside an Eulerian cell by a single straight line connecting the points of intersection of the boundary with the sides of the cell. It is possible to conceive of situations where the boundary winds in and out of a single cell creating some ambiguity. However, this occurs only when there are an insufficient number of zones to accurately calculate details of the flow. Therefore it is assumed that the Eulerian zoning is always fine enough so that the boundary has only two intersections with each cell. Having broken the boundary into a set of straight line segments, each associated with a unique Eulerian cell, one can specify the position of each segment by a unit vector normal to the boundary segment positioned at the midpoint of the segment. HOPI uses the convention that the normal points towards the liquid and to the left as one advances from the ith to i + 1th boundary point.

The second step is to define and flag Eulerian boundary cells as those along the inside edges of the contour approximated by the boundary segments. The liquid area of the boundary cells are then calculated again using the convention that the liquid is to the left as one advances from the ith to i + 1th boundary point. Then, if the liquid fraction of the total cell area is greater than 1/4, the boundary cell flag, OB, is turned on. If the liquid area fraction is too small the cell is flagged COR. It is then determined to which of the four neighboring cells the boundary segment normal points nearest and then set the boundary flag, OB, for that cell. When that cell also contains a boundary segment the two segments can be replaced with one by removing the boundary intersection point between the two adjoining cells. This new segment, spanning two cells, is also defined by velocity and position vectors at its midpoint. This case is illustrated in Figure 5. Note that as a result of this selection process the midpoint of a boundary segment may not physically lie in the Eulerian boundary cell with which it is associated. Thus, it is sometimes necessary to assign a pointer to a boundary cell indicating which neighboring cell contains the midpoint of the associated boundary segment. Once the boundary cell flags have been set it is necessary to go through them and turn off the boundary (OB) flag in any cell in the corner of a right angle cell pattern, since such cells are bounded on two adjacent sides by either a pair of interior or exterior cells and on the other two by boundary cells. Figure 6 shows a closed boundary curve, the approximate Eulerian boundary, and the cell pattern. It illustrates the various cases mentioned above.

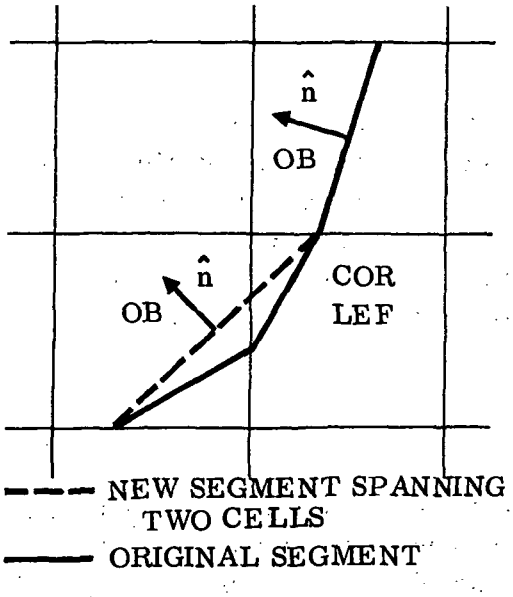

Figure 5. Replacing Two Boundary Segments With One Segment Spanning Two Cells

This process of defining a set of Eulerian boundary cells is analogous to the defining of a set of free surface cells in the MAC method but with the additional constraint that the resulting cell pattern avoids overdetermining the boundary condition on the pressure. Cells just outside the Eulerian boundary are flagged as COR cells while the remaining cells outside the Eulerian boundary are flagged as external (EXT) cells. This is so that one can tell when velocity components lie on the exterior sides of boundary cells.

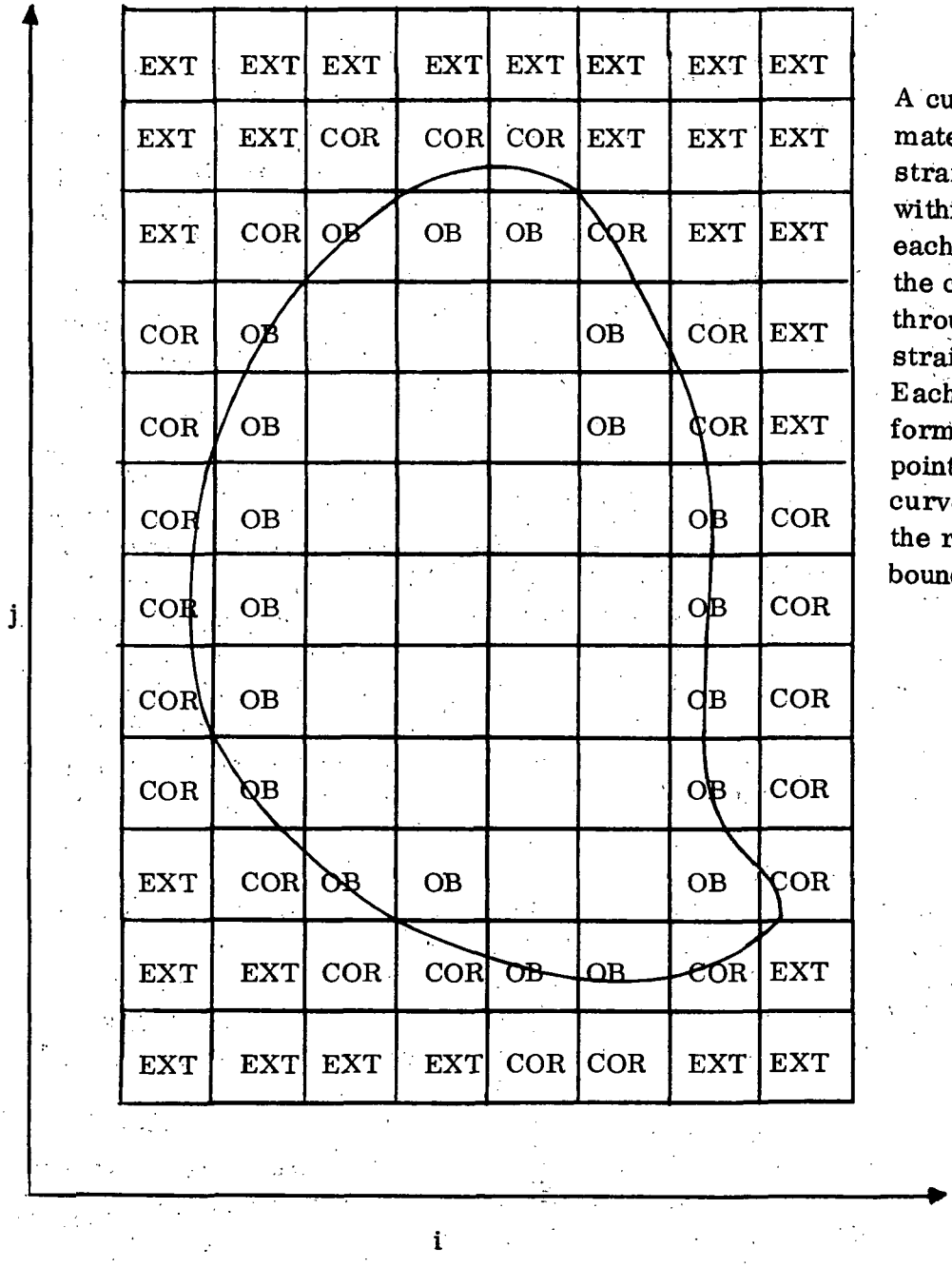

NOTE

A curved wall is approximated by a series of straight line segments within the grid mesh, where each cell that has part of the curved boundary passing through it contains a straight line segment. Each line segment is formed by joining the two points formed where the curved boundary crossed the rectilinear Eulerian boundary of the cell.

Figure 6. Permanent Cell Flags for Arbitrary Boundary

Once the boundary cells (flagged - OK) have been determined, the following relaxation equation is used to compute the pressure in these cells:

$$\psi_{ij}^{k+1} = \psi_{ij}^{k} - \frac{RELAX}{\lambda} \left[\left(V_p^{n+1} \right)^k \cdot \hat{n} \right]_{ij} \tag{8}$$

In this equation $\hat{n}$ is the normal defining the boundary segment associated with cell (ij) and $(V_p^{n+1})^k$ is the liquid velocity at the midpoint of the sgement computed with the MAC area weighted interpolation formula as shown in Figure 7.

Clearly $(V_p^{n+1})_{ij}^k$ is one of the iterates and must be recomputed each time the pressures and velocities are adjusted. The relaxation parameter and minimum mesh dimension are RELAX and λ respectively. The formula shows that instead of adjusting the pressure proportional to the divergence or net flux out of a cell one adjusts it proportional to the flux across the boundary measured relative to coordinates fixed in the boundary. If liquid is flowing across the boundary the pressure will be increased until the outflow stops. Conversely, if liquid is tending to separate from the boundary the pressure will decrease until the liquid flows tangent to the boundary.

Velocities at the exterior sides of the Eulerian boundary cells and other exterior points are necessary in the area weighting formula, and must be recomputed during each iteration sweep. These velocity components are determined in the same way as those on the open sides of free surface cells in the MAC method. In Figure 8 representative sections of boundary are shown in more detail. The original Lagrangian boundaries are indicated by dotted lines, and the resulting boundary segments and normals are shown. Heavy dark lines outline the outer edges of the boundary cells. The values of the velocity components at the edges and outside the Eulerian boundary, where necessary, are given in terms of their interior neighbors for the 2-dimensional plane case. In 3-dimensions with axial symmetry radius factors would be necessary to preserve continuity.

In addition to calculating new cell pressures during each cycle of iteration one must also recalculate the velocity components. During each iteration the sum of the old velocity component at time $n\Delta t$, the advection and the viscous terms are stored in $\tilde{u}_{i+1/2,j}$ and $\tilde{v}_{i,j+1/2}$ which need to be computed only once. Changes in the new cell velocity iterates then depend only on changes in the gradient of the pressure iterates.

In HOPI the pressures of arbitrary boundary cells are located at the boundary. This requires that one interpolate to find the cell centered pressure to use in the momentum equation. Figure 9 illustrates the method of linear interpolation. A real advantage of the simultaneous iteration method and Equation 8 is that it gives a simple automatic way of including complicated boundary conditions.

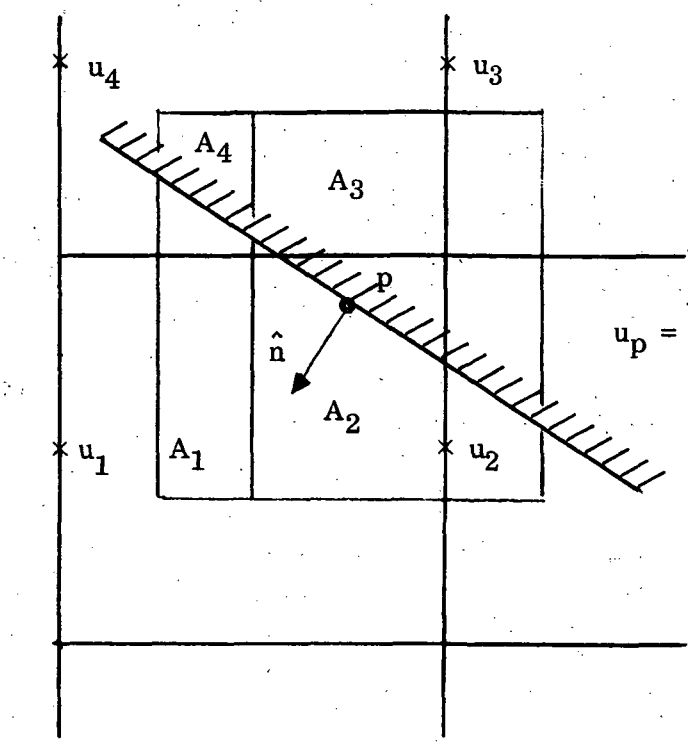

u COMPONENT V_p

$$u_p = \frac{A_1u_1 + A_2u_2 + A_3u_3 + A_4u_4}{A_1 + A_2 + A_3 + A_4}$$

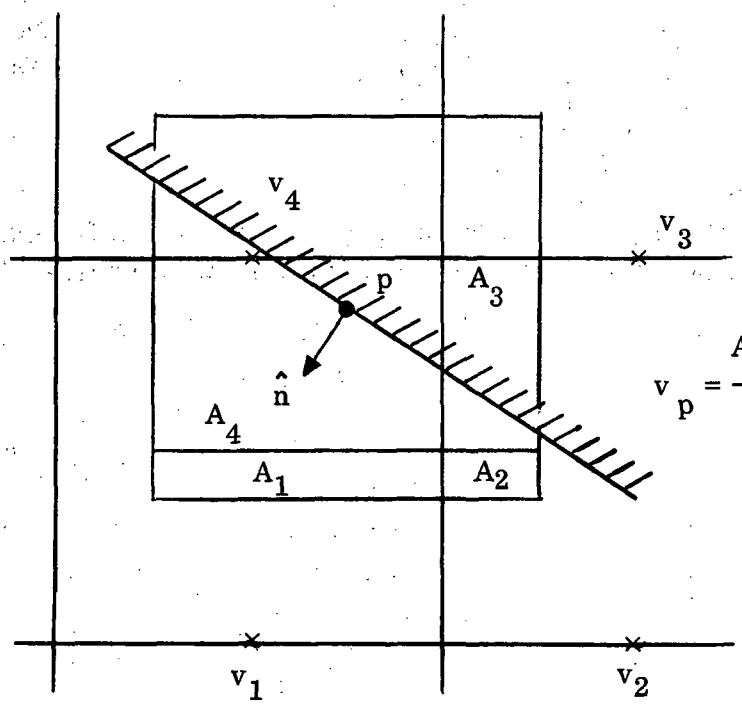

v COMPONENT of V_p

$$v_p = \frac{A_1v_1 + A_2v_2 + A_3v_3 + A_4v_4}{A_1 + A_2 + A_3 + A_4}$$

Figure 7. Interpolating Scheme for Obtaining the Liquid Velocity at the Midpoint of A Boundary Segment

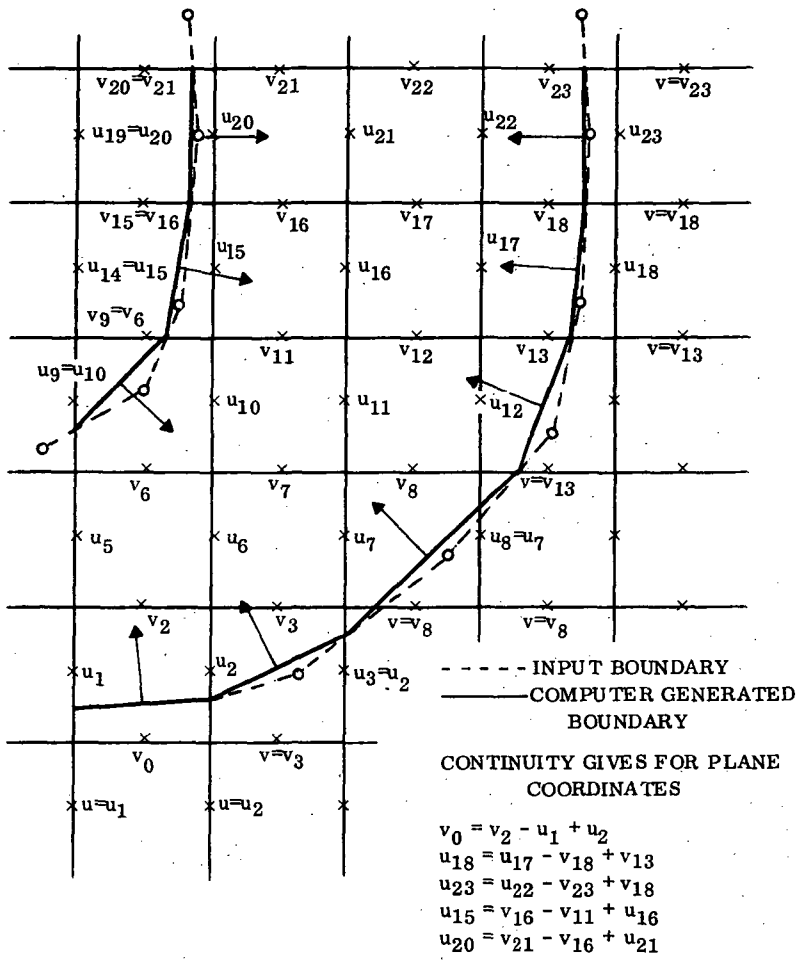

Figure 8. Determination of Mesh Velocities on the Exterior Sides of Eulerian Boundary Cells and Assignment of Boundary Segment Normals

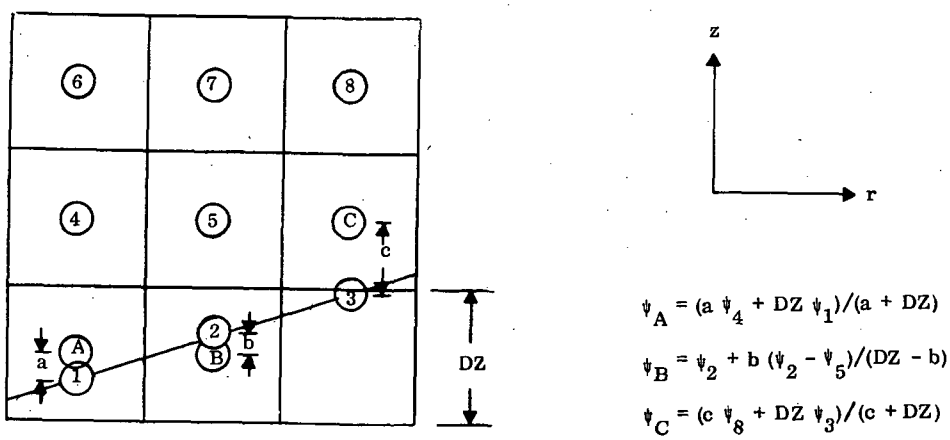

Figure 9. Pressure Interpolating Scheme

The marker particles, which are typically input at a density of at least four per cell, specify the fluid configuration with an uncertainty much less than the Eulerian mesh width. Because of this some finer criteria other than just the knowledge that a boundary cell contains particles is necessary. We require in addition that

$$(\vec{X}_p - \vec{X}_n) \cdot \hat{n} < \epsilon \lambda$$

where $\vec{X}_p$ is the particle position, $\vec{X}_n$ is the position of the midpoint of the boundary normal, $\hat{n}$ is the boundary normal, and ϵ is some fraction of the cell width λ typically 1/4. Thus, we do not begin computing a pressure in boundary cells until the particles come within $\epsilon \lambda$ of the boundary segment.

When free surfaces are present we also need to know how to treat cells containing the intersection of curved wall boundaries and free surfaces. The pressure at the intersection point should be equal to the ambient pressure, but because the pressure is defined only on the Eulerian net, it is sometimes not possible to zero the flux at the boundary consistent with vanishing divergence without introducing a pressure. This happens when the angle between the free surface and the boundary is small and the liquid is colliding with a wall, producing a liquid layer on a scale too fine to be resolved by the Eulerian mesh. We define an intersection cell to be one that contains liquid and has one or more empty interior or pressure surface neighbors, and one or more exterior neighbors. When this definition is satisfied, the pressure is set equal to ambient pressure and the velocities are adjusted directly. In most circumstances the liquid in the cell will be part of a much larger mass. When there are one or two liquid neighbors, the velocity components at the sides in contact with the liquid are preserved, and those at the open and boundary sides adjusted to make the velocity tangent at the boundary consistent with vanishing divergence. In the case of one liquid neighbor, the velocities at the opposite cell sides are assumed equal, and the component with both sides open or boundary is adjusted. In either case the flux at the boundary is a linear function of a single variable, and the zero is easily found. If the velocity at the boundary is initially directed away from the boundary, nothing need be done. The remaining possibility is that there are no liquid neighbors, as happens when a small isolated element strikes the boundary. In this case we set the component of the particle velocity normal to the boundary equal to zero, and preserve the tangential component. If a gravitational force is present we accelerate the particle velocities by the component of the gravitational vector tangent to the boundary. This is a free slip condition.

2.2.6 CALCULATIONS TO PLANE COORDINATES. The equations in HOPI are all written in cylindrical coordinates, but the program is arranged so that the calculations can be performed in plane coordinates with a minimal loss in computing efficiency.

The geometry type is specified by the user through the input quantity PC, which equals 0.0 for calculations in cylindrical coordinates, or 1.0 for calculations in plane coordinates. For plane coordinates, δx is input in place of δr and δy in place of δz. From this point on, HOPI performs the transformation automatically in the following manner.

The equations contain coefficients involving the use of r_i, the radius to the center of cell i, and $r_{i\pm1/2}$, the radius of right and left edges of cell i. To avoid recalculating these radii each time they are encountered, HOPI generates a number of tables which are entered with the index i for the quantities $r_{i+1/2}$, r_i, $1/r_{i+1/2}$, $1/r_i$, $(4r_i - \delta r)/(4r_i + \delta r)$, and $(4r_i + \delta r)/(4r_i - \delta r)$. If plane geometry is specified by PC, however, every entry in all six tables is generated as unity, causing all radial effects to disappear. Further, PC itself directly appears in some of the equations. For example, an expression applicable only to cylindrical coordinates is multiplied by (1.0-PC), forcing its cancellation in plane coordinates.

2.2.7 PROBLEM SETUP. Data punched on input cards provide the setup routine with the information required to generate the flow field at initial time. Basic requirements are the number of interior cells in both directions ($\bar{I}$ and $\bar{J}$), the geometry (cylindrical or plane), the size of each cell (δr by δz or δx by δy), the initial layout of marker particles specifying the number of particles for each cell, and the initial u's and v's for those cells containing particles. Other necessary information is included that specifies the boundary types on the four sides of the mesh, the location of an obstacle if one is present, the fluid viscosity, the amount of gravitational acceleration, the time step (δt), and the intervals at which plots or prints are to be made.

In the HOPI set up, the mesh is initially flagged as all EMP cells, surrounded by BND cells. If an obstacle is present, its cells are permanently flagged OB. Cells outside OB cells are permanently flagged either COR or EXT. Subsequently, any cells containing particles are flagged FUL. At this point, a set up containing a free surface has no SUR cells, but this is remedied immediately in the first calculational cycle when the cell flags are adjusted.

Finally, the setup routine must calculate scaling parameters for the microfilm plots that will be made of the marker particles, and calculate various coefficients and tabular data that will be used repeatedly in the calculational cycle.

At this point, the setup ends and control passes to the first calculational cycle. Omission of any variables, such as SUR cell flags, tangential velocities in BND cells and on the free surface, is rectified in the first cycle, because their calculation is a standard part of every cycle.

3.0 RESULTS AND DISCUSSION OF RESULTS

During this contract five liquid reorientation cases were run using the computer program discussed in Section 2. Three of the cases simulated actual NASA LeRC drop tower test conditions and were used to give confidence in the results generated by HOPI. The additional two cases simulated full-scale Centaur tank conditions.

3.1 CORRELATION OF ANALYTICAL RESULTS WITH TEST DATA AND THEORY

Three analytical runs were made which corresponded to actual LeRC drop tower test. These runs were used to help establish the accuracy and limitations of the existing code to solve typical liquid reorientation problems. All three problems had the following characteristics:

- Height to diameter ratio of 2
- Cylindrical tank with a radius of 7 cm
- Fluid (FC-78) had a kinematic viscosity $\upsilon = 4.74 \times 10^{-3}$ cm^2/sec (Ref. 12)
- Initial interface shape corresponding to an initial bond number of 10
- Hemispherical forward dome
- Initially the fluid was at rest (all velocities = 0)
- Grid mesh of DR = DZ = 1 as indicated in Figure 10
- All boundaries were input with the free slip condition (Section 2.2.5)

In all plots shown in this section just half of a tank is shown due to symmetry. The left side of each plot corresponds to the center of the tank.

CASE 1. Case 1 had the following additional characteristics:

- 20% liquid (by volume)
- Spherical segment bottom dome
- Settling acceleration (GZ) of 31.4 cm/sec^2
- Turbulent viscosity coefficient = 0.0
- Initial Marker particle density = 4 × 4 per cell (580 particles)

Figures 11A through 11C give computer generated SC 4020 plots of the Marker particles. Figures 12A through 12C give computer generated SC 4020 plots of the velocity vectors at selected times. Initially the fluid was at rest (all velocities = 0). It is noted that in Figure 12A certain regions which contain fluid do not have a velocity vector indicated. This results since the velocities must be larger than a certain minimum value to be printed as a SC4020 velocity vector.

The results agree closely to those of actual test data supplied by NASA LeRC. The liquid flows down along the side of the cylinder with a velocity $V = .87 \times g_z \times t$

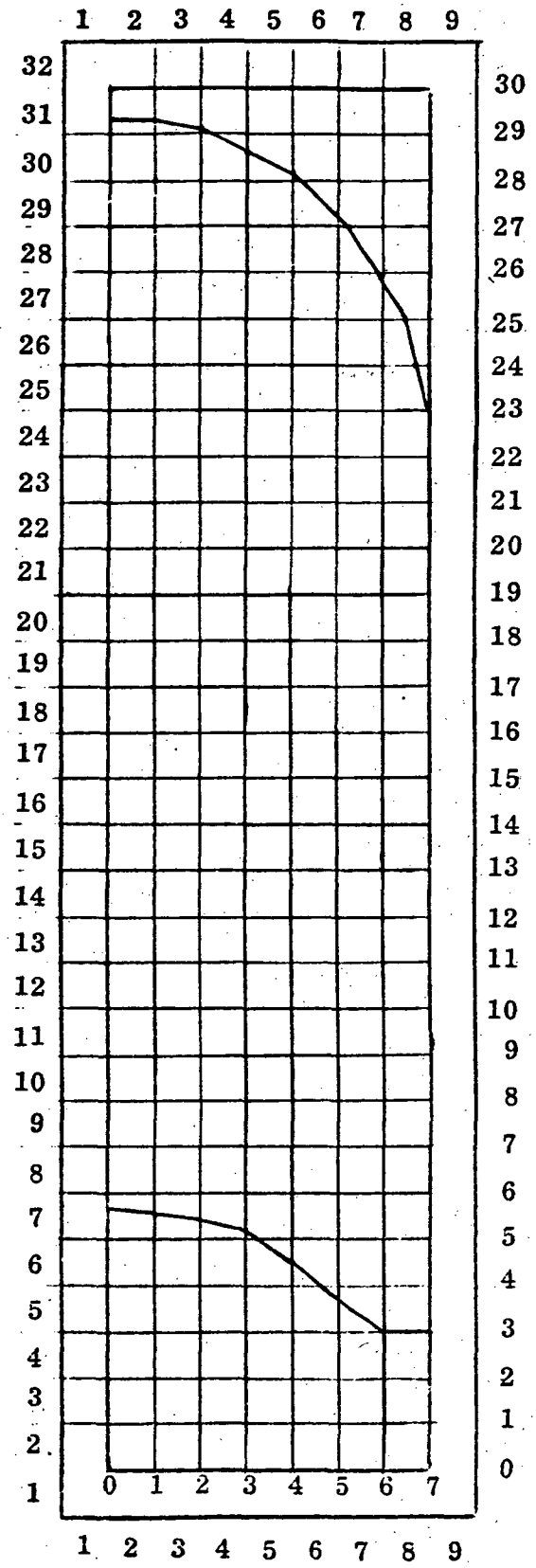

Figure 10. LeRC Drop Tower Test Simulation With Grid Mesh of DR = DZ = 1 Cm

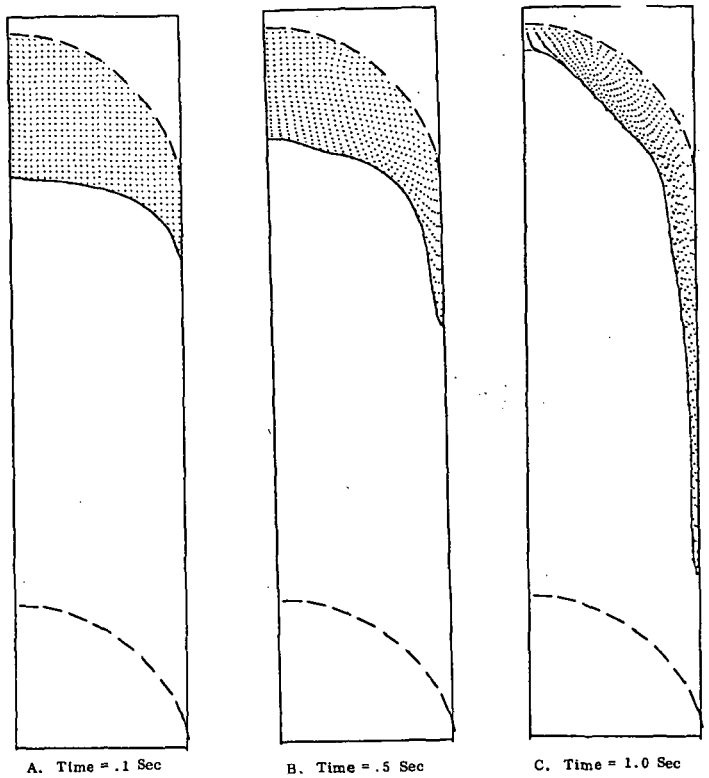

Figure 11. SC 4020 Marker Particles Plot for Case 1

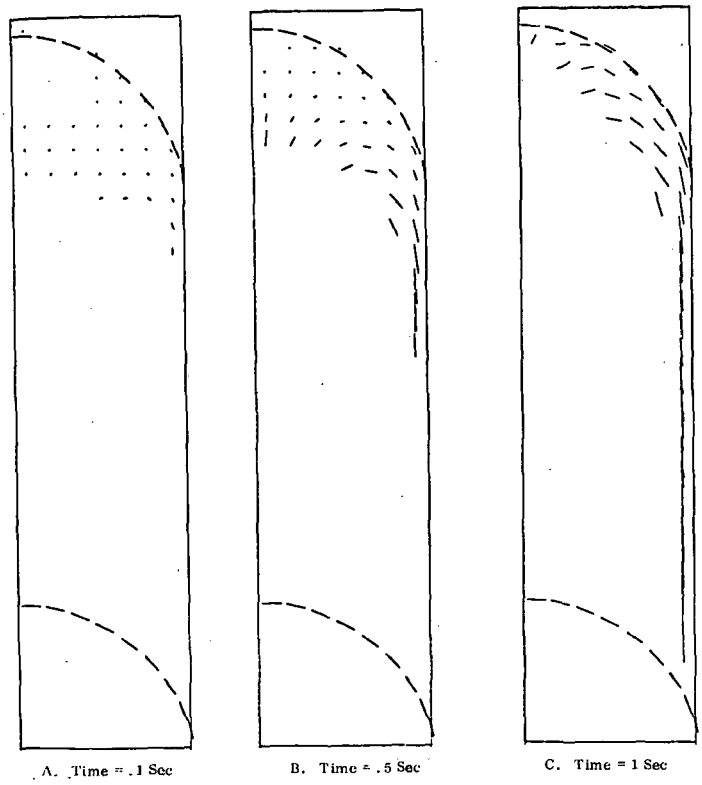

Figure 12. SC 4020 Velocity Vector Plots for Case 1

(Reference 2) where t is the time duration that the settling g-load is applied. The liquid in the center of the tank moves up toward the top bulkhead and the fluid adjacent to the top bulkhead moves parallel to the bulkhead as indicated by the velocity vectors in Figure 12C.

CASE 2. Case 2 had the following additional characteristics:

- 70% liquid
- One cell truncated spherical segment bottom dome
- Settling acceleration of 31.4 cm/sec^2
- Turbulent viscosity coefficient = .05
- Initial Marker particle density = 6 × 6 per cell (4285 particles)

This problem was run for approximately 2.4 seconds of settling time. Some problems which did not occur in the first run appeared. The first problem was at the corner where the fluid coming down the wall impinged on the bottom dome. It was found necessary to truncate the dome by at least one cell since, for the present grid size, the program could not resolve the fluid motion. This is illustrated schematically in Figure 13. Figures 13A and 13B are the corner without and with one cell truncation respectively.

The vector arrows indicate the motion of the fluid. In Figure 13A it is seen in cells 8, 4 and 8, 3 that the fluid moves in two different directions. Since for a given cell there is only one set of velocity for all the particles in the cell, the two velocities cannot be resolved.

This problem can be corrected by using a smaller grid mesh. However, since the present coding does not allow for variable grid sizes, the finer grid size needed would greatly increase the running time of the problem.

A second problem also developed when the test case was run past the point of initial impact with the bottom dome. The problem was in the surface definition as defined by a subroutine called SURP. SURP has two main functions: one is to evaluate surface tension forces, the second is to extrapolate the pressures as calculated at the surface to find the appropriate pressure for the center of the surface cell. Figures 14A and 14B illustrate how the surface becomes defined along the arbitrary boundary. This results since the particles that initially hit the bottom stagnate while the particles that follow move across the boundary. Because of this phenomena it is an inherent limitation of the program that subroutine SURP cannot be used once a condition like this exists.

The first approach to solving this second problem was to delete all surface marker particles. However, as shown on Figure 15A this resulted in an instability in the surface. The second approach consists of deleting surface marker particles as they entered cells containing segments of an arbitrary boundary. As indicated in Figure 15B the instability is gone. It is therefore recommended that this second approach be used.

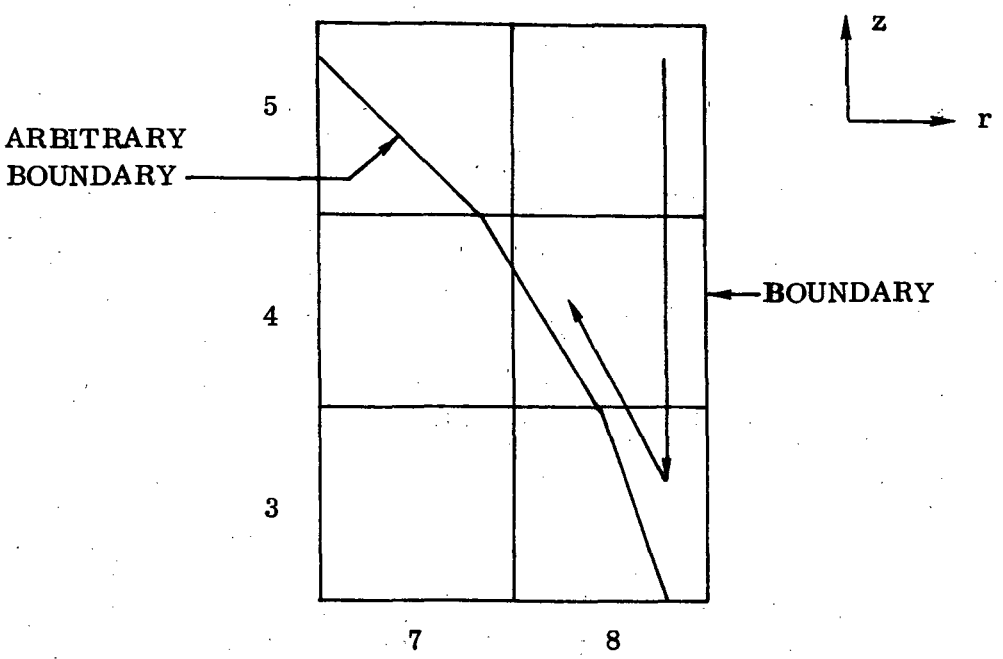

A

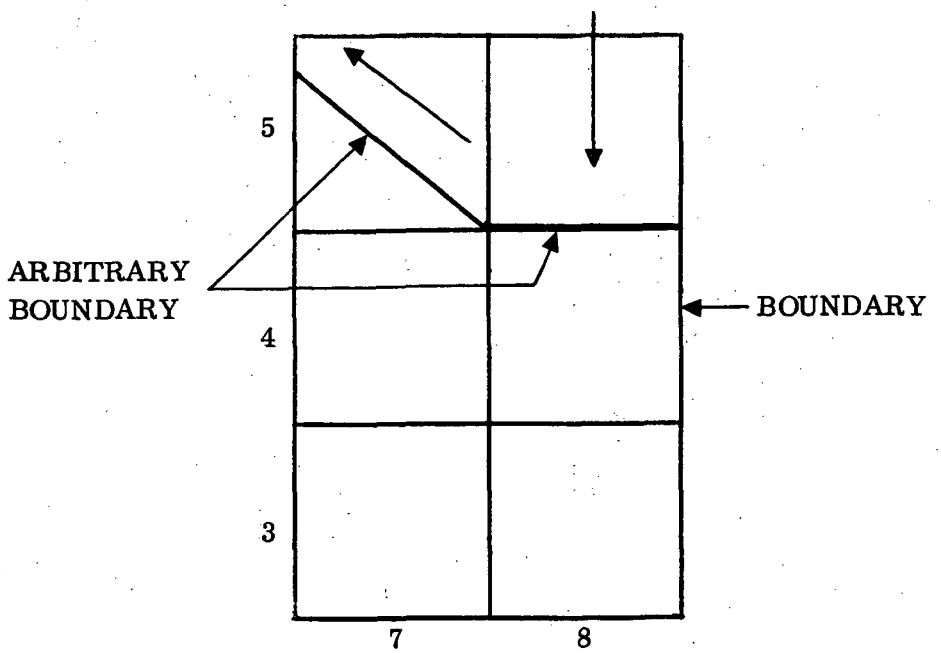

B

Figure 13. Magnified Section of Grid Network Showing Cells Containing Arbitrary Boundary Segments

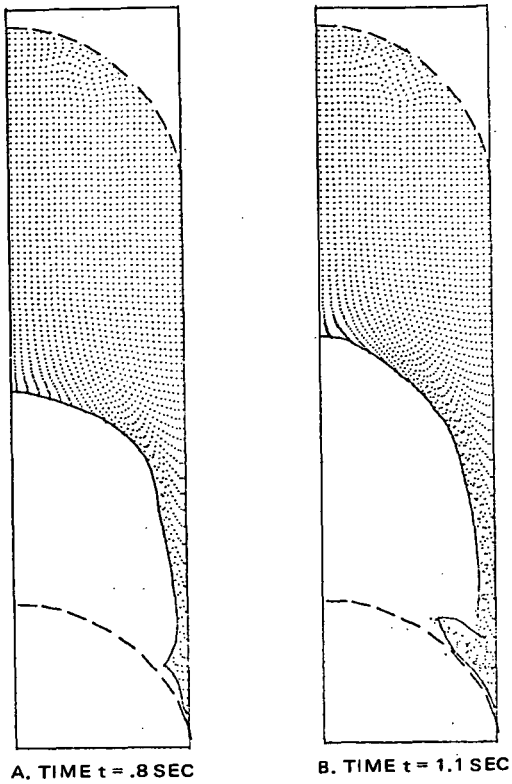

Figure 14. Surface Definition After Impact of Fluid on Arbitrary Boundary

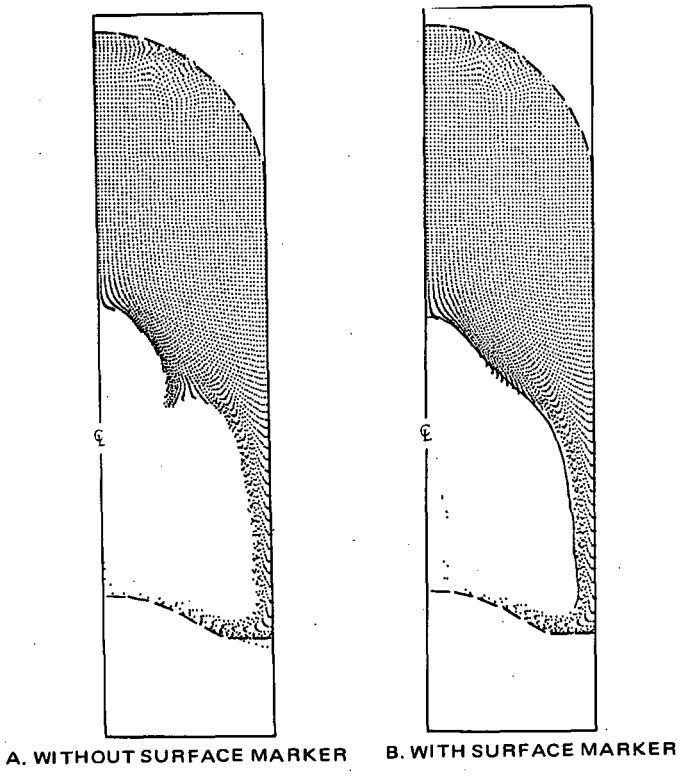

Figure 15. Effects of Surface Marker Particles in Ullage Section for Test Model With 30% Ullage at 1.05 Seconds

An examination of the geyser that has formed on Figure 15B illustrates another problem: a condition of rarified particles. This problem results when the particles are accelerating along the bottom boundary. This acceleration results when fluid is moving in toward the center of a cylinder under its momentum. As the radius of the cell containing fluid decreases, the radial component of velocity in that cell increases inversely with the radius.

The condition of rarified particles becomes a problem when a cell that should contain particles does not. This is the case in the geyser seen in Figure 15B. A subroutine (called ADPART) was written to remedy this problem. Figure 16 shows a typical geyser with the additional particles as added by subroutine ADPART.

Also while running Case 2 the turbulent viscosity coefficient (TURB) was varied to determine its effect on the fluid motion (Section 2.1). Figure 17 shows the basic fluid motion at approximately 1.1 sec for three different values of TURB. It is clear that the lower the value of TURB the faster is the velocity of the fluid and hence the sooner the geyser begins to form. It is emphasized that the turbulent viscosity is calculated in a cell containing fluid when at least two of its adjacent neighboring cells also contain fluid. This criteria is needed so that $\partial u/\partial z$ and $\partial v/\partial r$ can both be computed. Unfortunately due to the coarse grid mesh this condition is not always satisfied when in reality it should be. This is true when the fluid is sliding down the wall and is moving across the bottom boundary as a layer of fluid with a thickness less than the grid dimension. While this condition exists for a relatively short duration during Case 2, this problem will become more severe during the remaining cases.

Since the lack of a surface pressure interpolation scheme has been shown to result in surface instability (Figure 15), it was concluded that it is necessary to maintain the surface pressure interpolation scheme during geyser formation. Also, to minimize surface breakup in the geyser itself it is necessary to add surface marker particles over the entire surface to include the geyser. Therefore, a subroutine was written to internally add the necessary surface marker particles at selected times. Figure 18 shows a case where the subroutine was used to add particles.

Figures 19A through 19L give computer generated SC4020 plots of the Marker particles for Case 1. The surface pressure interpolation scheme was discontinued at 1.566 seconds. This is the reason that plots 19G through 19L have no solid line outlining the surface as is the case in plots 19A through 19F. Figures 20A through 20C give computer generated SC4020 plots of the velocity vectors at selected times.

Figure 21 gives photographs of the drop tower test results simulated by Case 2. Initially the interface shape corresponds to a Bond number of 15. The test model was a scaled model of the current Centaur tank. Except for the deviation in the initial interface shape and the fact that the model had minor differences in tank end shapes, the remaining characteristics of settling acceleration, fluid properties, and percent liquid are the same as outlined for Case 2. All the times associated with each photograph in Figure 21 are rounded off to the nearest tenth of a second.

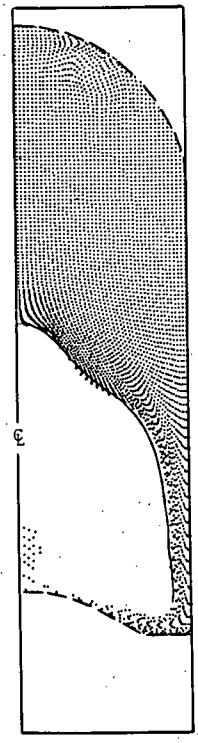

Time = 1.025

Figure 16. Test Model With 30% Ullage With Particle Addition by Subroutine ADPART

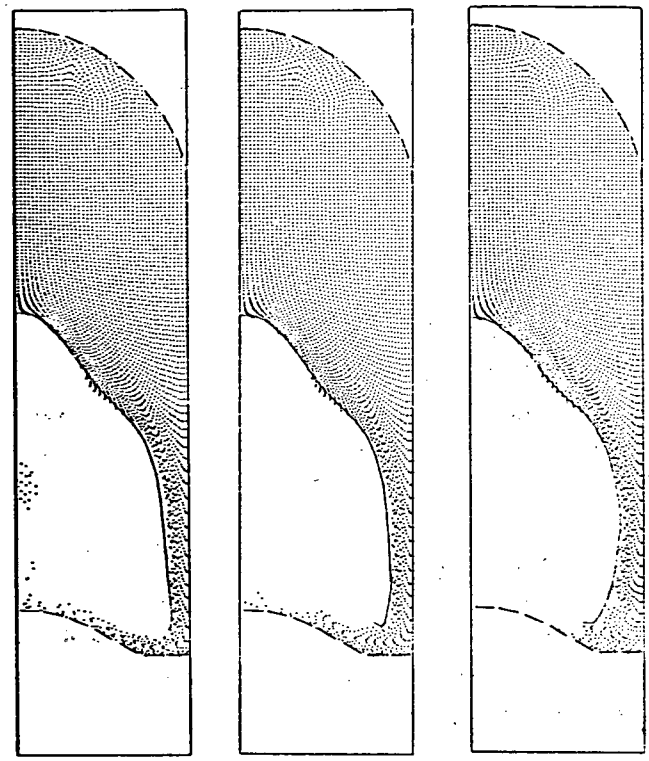

A. TURB = 0 B. TURB = .1 C. TURB = 1.0

Figure 17. Test Model at Approximately 1.1 Second for Various Values of TURB

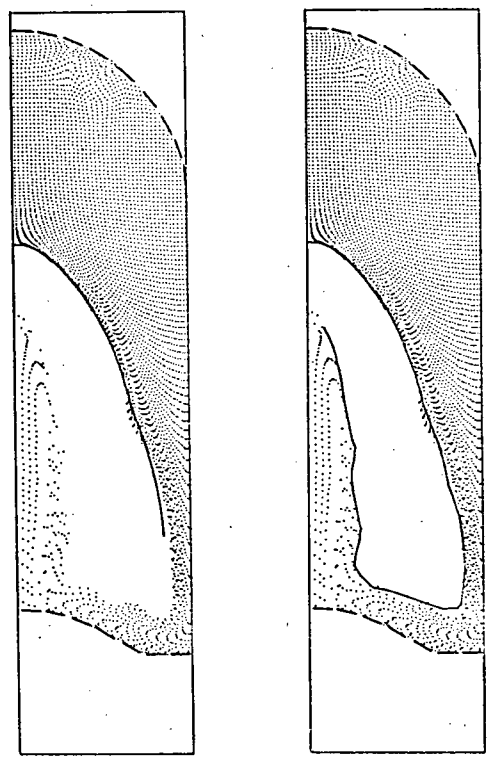

A. Without Added Surface Marker Particles

B. With Added Surface Marker Particles

Figure 18. Test Model at Approximately 1.375 Seconds With and Without Added Surface Marker Particles

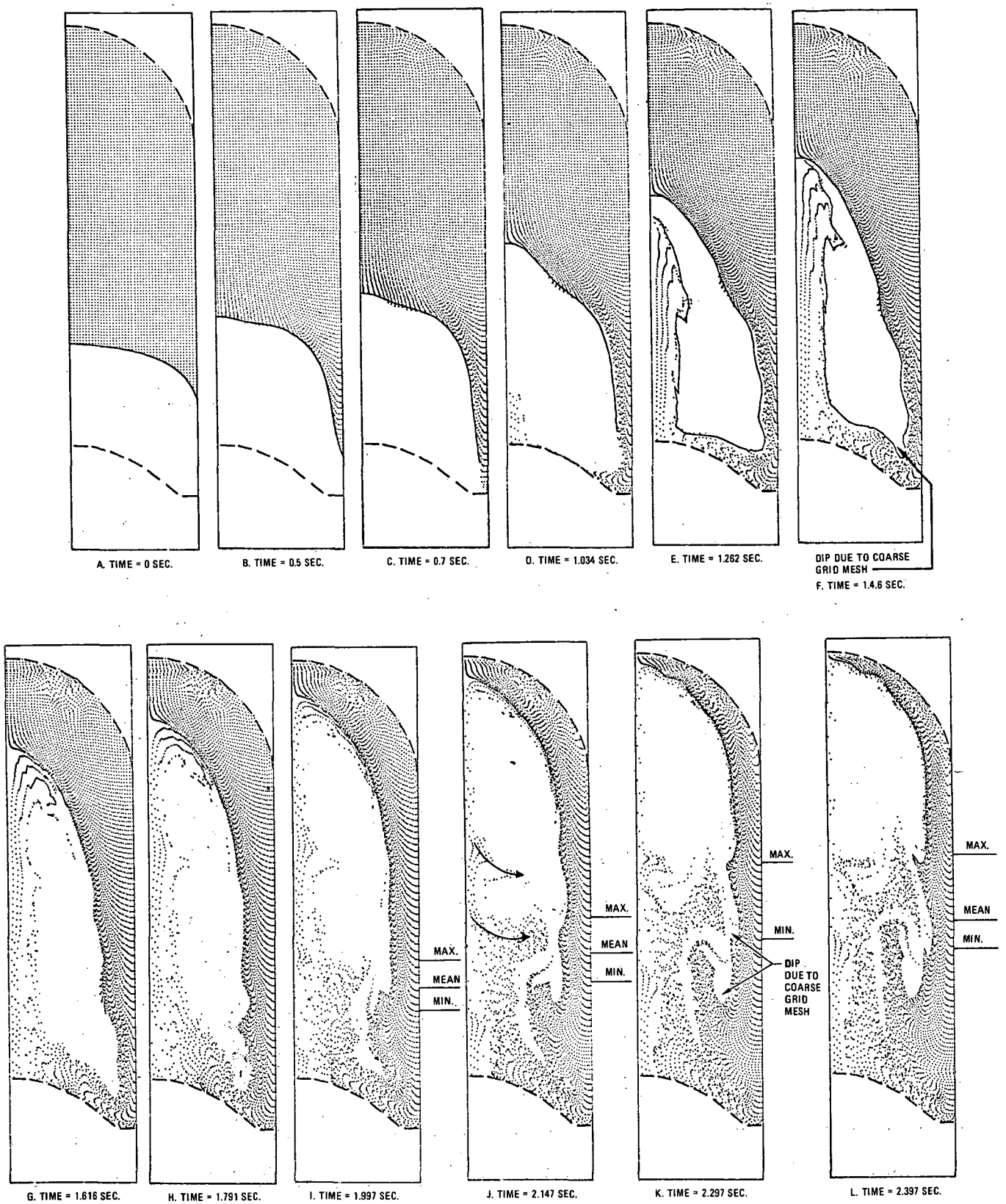

Figure 19. SC4020 Marker Particle Plots for Case 2

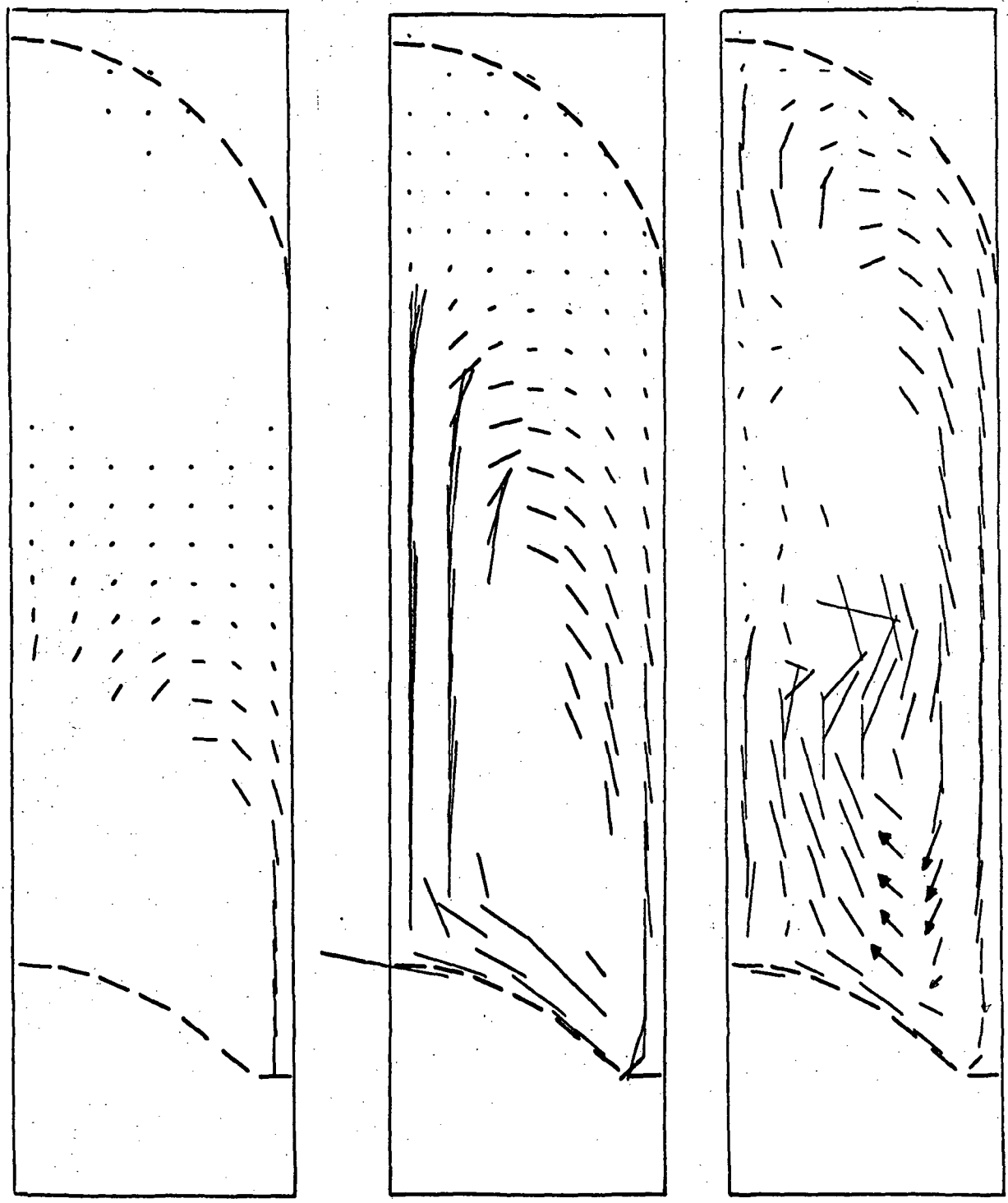

A. Time = .600 Sec B. Time = 1.366 Sec C. Time = 2.047 Sec

Figure 20. SC4020 Velocity Vectors Plots for Case 2

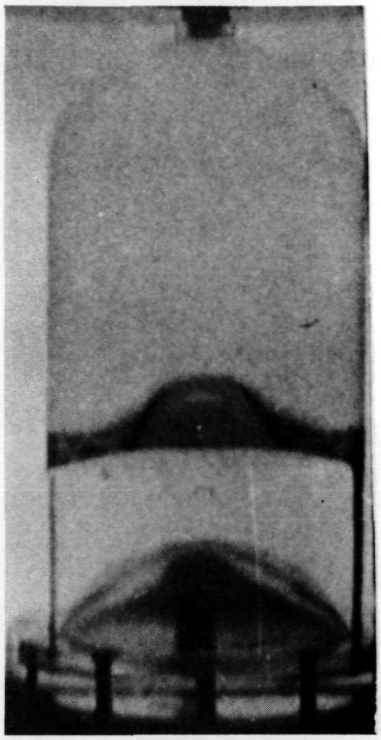

A. Time = 0

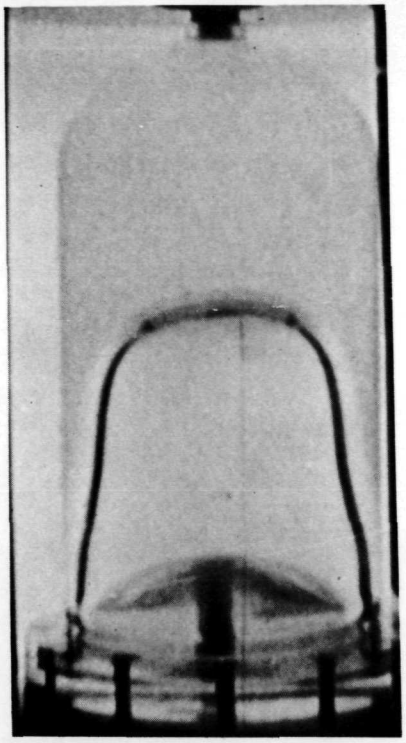

B. Time ≈.7 sec.

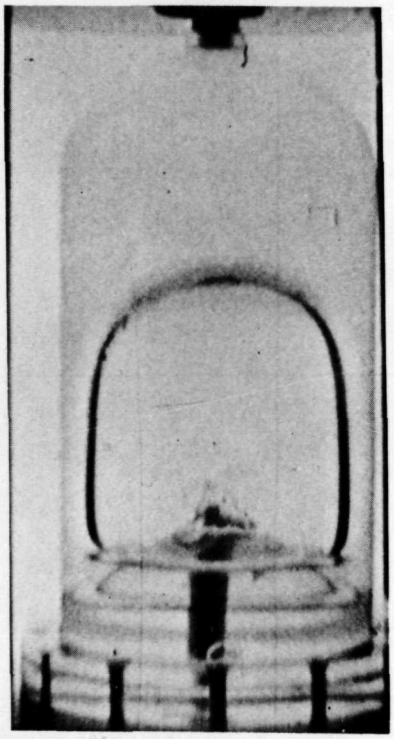

C. Time ≈ .9 sec

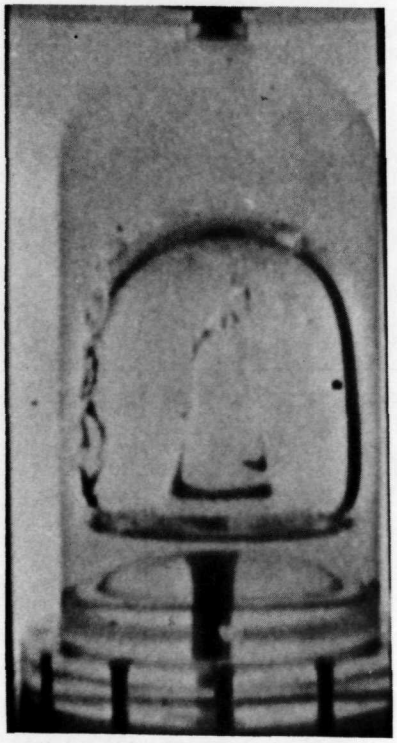

D. Time≈1.2 sec

Figure 21. Photographs of Drop Tower Test Results Simulated by Case 2

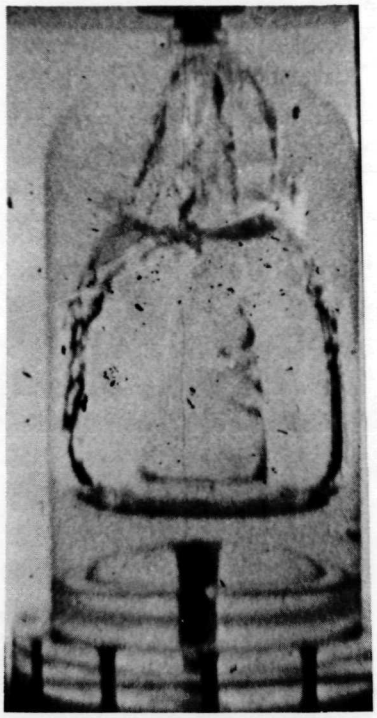

E. Time ≈ 1.4 sec

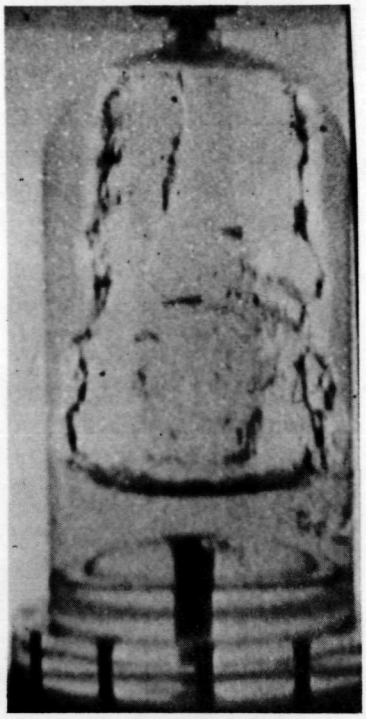

F. Time ≈ 1.7 sec

G. Time ≈ 2.1 sec

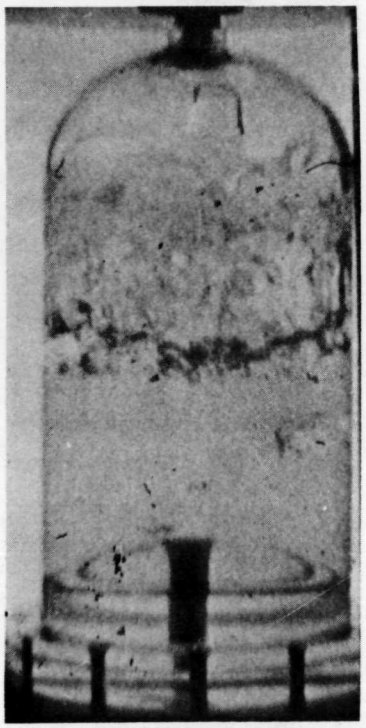

H. Time ≈ 2.4 sec

Figure 21. Continued

The analytically calculated motion was compared with actual drop tower test data supplied by NASA/LeRC. The following indicates the close degree of correlation.

- In both cases the liquid initially moves down the wall of the container with no Taylor instability appearing in the center of the tank. The liquid hits the bottom of the container at approximately 0.7 sec (compare Figure 19C with 21B).

- In both cases the liquid then moved along the bottom surface toward the center of the tank. The liquid does not separate from the bottom boundary.

- When the liquid reached the center of the tank a geyser formed as indicated in plot 19D. In both cases geyser formation began in less than one second (in .99 second for the analytical case and approximately .95 seconds in the test results).

- The geyser continued to rise and impinged on the fluid remaining in the upper portion of the tank. In both cases this impingement occurred in approximately 1.25 seconds (see Figure 19E). * In both cases the width halfway up the geyser is approximately 3.0 cm when it impinges the fluid in the upper region (see Figure 19E).

- In both cases the distance from the top of the tank to the free surface of the liquid in the top of the tank is approximately 10 cm when the geyser impinges the fluid in the upper region (see Figure 19E).

The correlation in the detailed fluid motion following geyser impingement on the fluid is not so accurate as above. In the test results the geyser actually pushes through the fluid in the upper region and hits the top of the tank at approximately 1.45 seconds. As can be seen in plots 19G through 19L the geyser does not push through the fluid to reach the top of the tank.

While the detailed motion after 1.25 second cannot be resolved by the program for the present grid mesh size it is felt that the lumped motion of the fluid is still accurate enough to give a good estimate of the "collected volume" for the duration of this problem. Also some other trends are noted.

- Beginning at about 2 seconds the geyser begins to collapse. This can be seen in velocity plot 20C. This collapsing of the geyser causes the liquid in the geyser to move as indicated by the arrows in Figure 19J. This same type of the geyser breakup is seen in the test results.

---

* As can be seen in Figure 19E there is a space between the geyser and the fluid in the upper region of the tank. However, as far as the program is concerned impingement has occurred since some of the geyser marker particles are in the same cell as the particles defining the surface of the fluid in the upper region.

- After approximately 1.7 seconds (Figure 19H) it becomes increasingly difficult to determine the true "collected volume." By the end of the problem at approximately 2.4 seconds there are a number of regions which appear to lack Marker particles (see Figure 19L). Does this actually imply entrained vapor as can be seen in the test results or is it a result of the course grid mesh causing inaccuracies in the fluid motion? Recall that once one marker particle gets into a cell the cell may be considered full of liquid for purpose of simulation. Also, the coarseness of the grid mesh causes the velocity vectors between two adjacent cells to deviate by over 90° in some cases. This is particularly true when the fluid coming down the tank wall hits the bottom boundary or the fluid on the bottom and is forced to change directions (see Figure 20C). The result is a dip in the fluid as indicated in Figures 19F and 19K. These dips should be neglected when determining the true "collected liquid volume." The lines to the right of some of the SC4020 Marker particle plot indicate the height of the liquid in the "collected volume. A basic criteria for estimating this height is given in Appendix A.

Up to approximately 1.416 second (Figure 19F) there is only one line indicating the "collected liquid" height. After that there are as many as three lines (if there are three the top implies maximum collected volume height while the lower implies the minimum collected volume height and the middle one implies the mean or estimated actual collected volume height). After seeing the LeRC test results, it is estimated that the true "collected liquid" height is between the minimum and the mean height while the region between this true height and the maximum height is a region which is filled with liquid and entrained vapor. Based on this assumption Figure 22 compares the analytical and experimental collected liquid height. It is noticed that the largest deviations occur during the initial part of the problem while after 2.0 seconds the analytical and test data agree almost exactly. Due to the ambiguity in any exact value for the true height (experimental as well as analytical) it is felt that the program does predict the "collected liquid" in this typical settling problem.

Figure 23 is the collected liquid volume corresponding to the collected liquid height in Case 22.

CASE 3. Case 3 had the following additional characteristics

- 20% liquid
- One cell truncated spherical segment bottom dome
- Settling acceleration of 70 cm/sec^2
- Turbulent viscosity coefficient = 0.05
- Initial Marker particle density 7 × 7 per cell

Figures 24A through 24F give computer generated SC4020 plots of the Marker particles The surface pressure interpolation scheme was discontinued at 0.90 sec (Figure 24E). It was found necessary to discontinue this interpolation scheme when the geyser

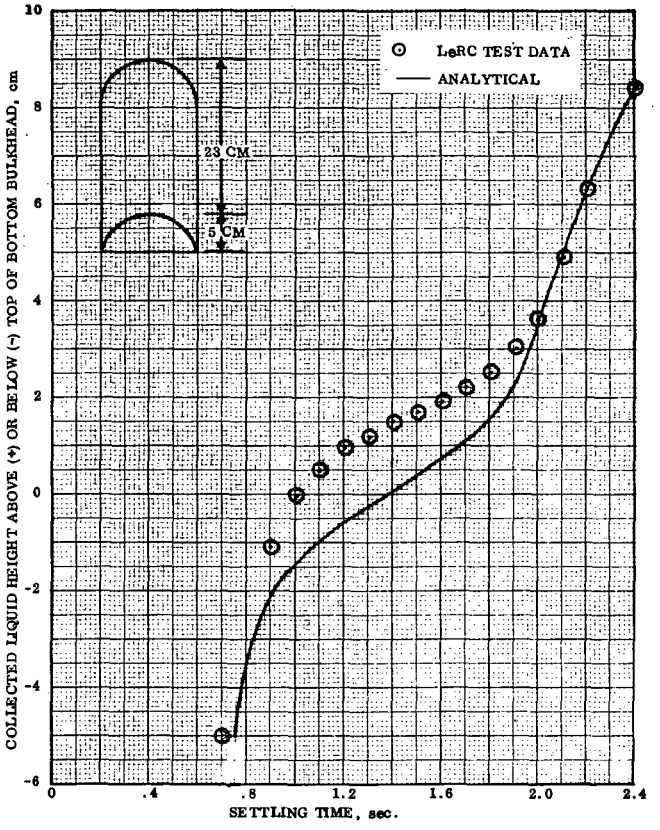

Figure 22. Comparison of the Analytical and Experimental "Collected Liquid"Height for Case 2

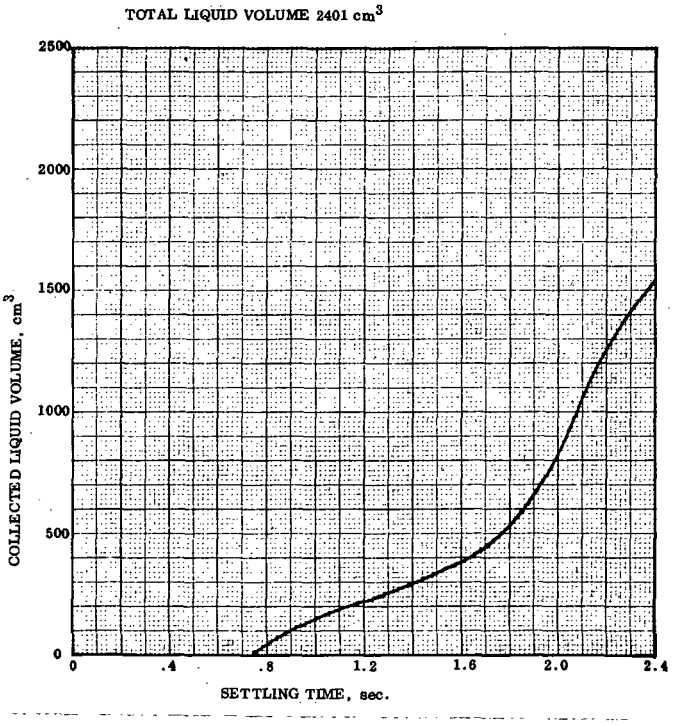

Figure 23. The Analytically Computed "Collected Liquid Volume" Versus Settling Time for Case 2

impinges on fluid remaining at the top of the tank. Figures 25A and 25G give computer generated SC4020 plots of the velocity vectors at selected times. Initially the fluid was at rest (all velocities = 0). The scale of the velocity vectors was changed after the initial geyser formation because the large velocities in the geyser would go off the plot at the initial scale. This is the reason why the velocity vectors of the fluid going down the wall are longer in Figure 25A than in 25B.

The results of this run correlated with actual drop tower test data and existing theory to the point of geyser formation. Figure 26 indicates how the leading edge velocity correlates to existing data (Ref. 2). The reason for the leading edge exhibiting a downward acceleration 13% less than freefall is basically because of the noslip condition which exists in real fluid flow problems (Ref. 7). However, during all the cases run during this contract the freeslip boundary condition exists on all boundaries. It is therefore concluded that the fact that the analytical leading edge velocity departs from the settling velocity and results in a close agreement with actual leading edge velocity is fortunate. The freeslip condition was used instead of the noslip condition since the grid mesh was too coarse to resolve the detailed motion of an actual boundary layer. However, the coarse grid mesh caused inaccuracies in the numerical computation which resulted in the deceleration of the leading edge. It is expected that with more accuracy, resulting from a finer grid mesh along the boundary, the leading edge acceleration would approach the settling acceleration if the noslip boundary condition continued to be imposed. The result would be that the leading edge velocity would be too high. If this occurs in future runs it is suggested that the HOPI code be modified so that a partial slip condition can be input for cases where the grid mesh is not fine enough for the noslip condition.

It was noted after running Case 2 that the leading edge velocity was slower than theoretically predicted. An examination of this code indicated that some velocities in empty cells were being prematurely deleted. This error was corrected before running Case 3. It is emphasized that the error was minor for Case 2 and that the basic conclusions developed from Case 2 still apply for Case 2.

The geyser forms initially at .840 sec. However, the geyser velocity was faster than in the drop tower experiments and once the geyser did hit the top of the tank the fluid motion could not be accurately resolved. The reason the fluid motion in the 20% liquid case cannot be accurately resolved can be seen by comparing Figure 24E with Figure 10. At this point the fluid is within thin sheets along the top bulkhead, the side wall, the bottom bulkhead and in the geyser. In fact the sheets are thinner than the cell width thereby causing almost all the fluid to be within surface cells. This means that the grid mesh is not fine enough to resolve the motion. To obtain the necessary resolution to accurately solve this problem, with the constant grid mesh restriction that now exists in the code, would require at least reducing by half the grid size in both the radial and axial direction. This would push the core size of the computer to the limit and would more than double the computer time needed to sclve the problem.

It is therefore concluded that the code in its present form should not be used to solve this type of problem. It is recommended that a variable grid mesh option be added to the program so that smaller grids can be used where needed (such as around corners).

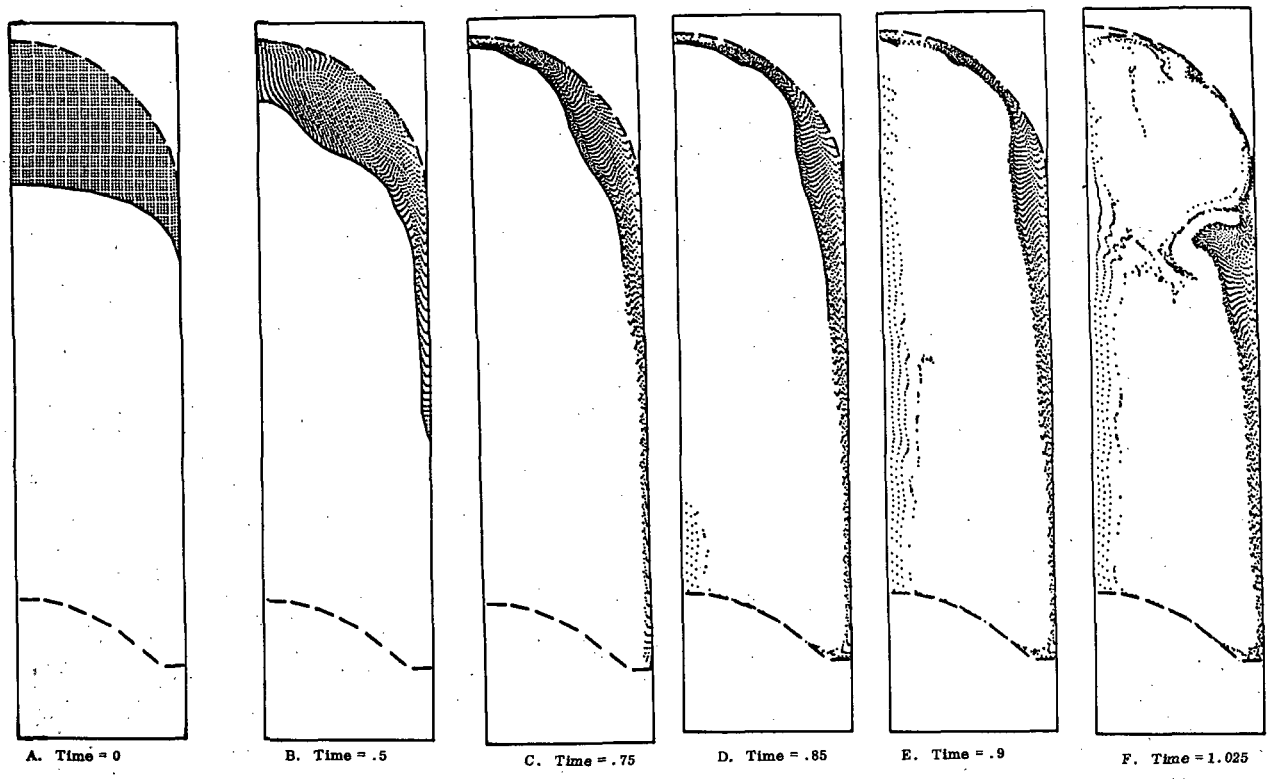

Figure 24. SC4020 Marker Particle Plots for Case 3

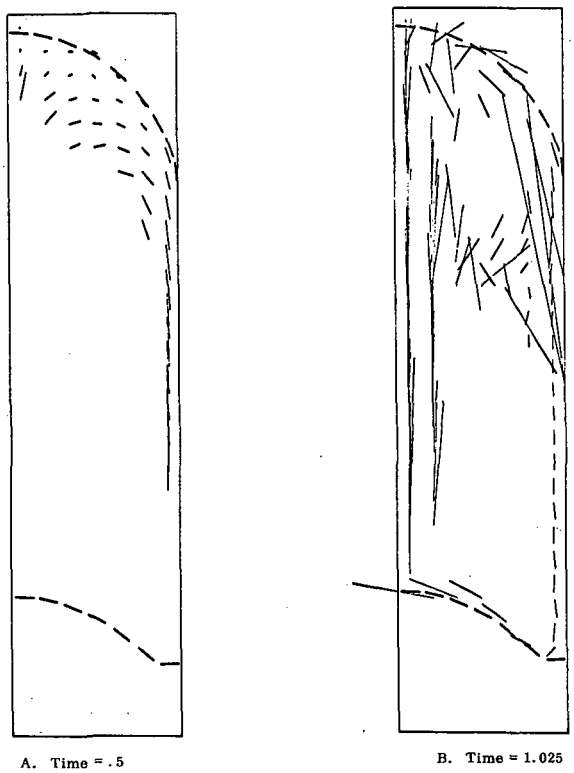

Figure 25. SC4020 Plots of Velocity Vectors for Case 3

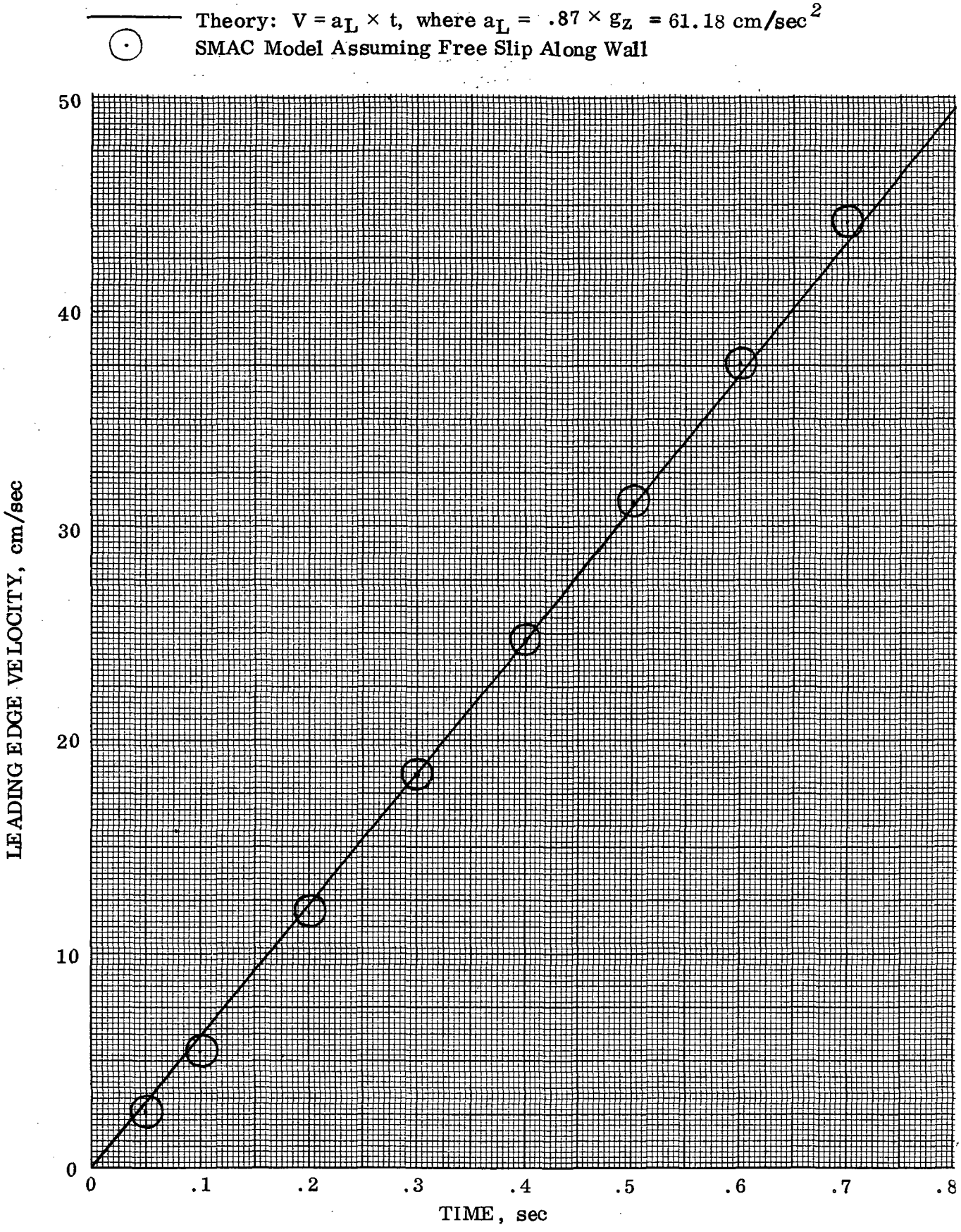

Figure 26. Correlation of SMAC Leading Edge Velocity With Theory for Case 2 (g_z = 70 cm/sec 2)

Conversely, large grids would be available in the same problem where detailed resolution of the motion is not so critical.

3.2 FULL SCALE TEST RESULTS

Two analytical runs were made to simulate full-scale Centaur fuel tank conditions. Both problems had the following identical characteristics.

- Height to diameter ratio of 2
- Cylindrical tank with a radius of 150 cm
- Fluid (LH_2) had a kinematic viscosity $\nu = 1.92 \times 10^{-3}$ cm^2/sec
- Initial interface shape corresponding to an initial Bond number, Bo of 10
- Hemispherical forward dome
- One cell truncated spherical segment bottom dome
- Initially the fluid was at rest (all velocities = 0)
- A grid mesh of DR = DZ = 21.425714 cm similar to that shown in Figure 10
- All boundaries were input with the free slip boundary condition (Section 2.2.5)

In all plots presented in this section just half of a tank is shown due to symmetry. The left side of each plot corresponds to the centerline of the tank.

CASE 4. The first full scale run (called Case 4) had the following additional characteristics.

- 70% liquid
- Settling acceleration of .27 cm/sec^2
- Initial Marker particle density 6 x 6 per cell (4285 particles)

Figures 27A through 27O give computer generated SC4020 plots of the Marker particles. The surface pressure interpolation scheme was discontinued at 50 sec. It has been found necessary to discontinue this interpolation scheme when the geyser impinges on fluid remaining at the top of the tank. Figures 28A through 28F give computer generated SC4020 plots of the velocity vectors at selected times. The scale of the velocity vectors was changed after the initial geyser formation because the large velocities in the geyser would go off the plot at the initial scale. This explains the longer velocity vectors of fluid going down the wall in Figure 28A compared with 28B.

CASE 5. The second full scale run (called Case 5) had the following additional characteristics.

- 85% liquid
- Settling acceleration of .135 cm/sec^2
- Initial Marker particle density of 5 x 5 per cell (3652 particles)

Figures 29A through 29N give computer generated SC4020 plots of the Marker particles. The surface pressure interpolation scheme was discontinued at 55 seconds. Figures 30A through 30F give computer generated SC4020 plots of the velocity vectors at selected times.

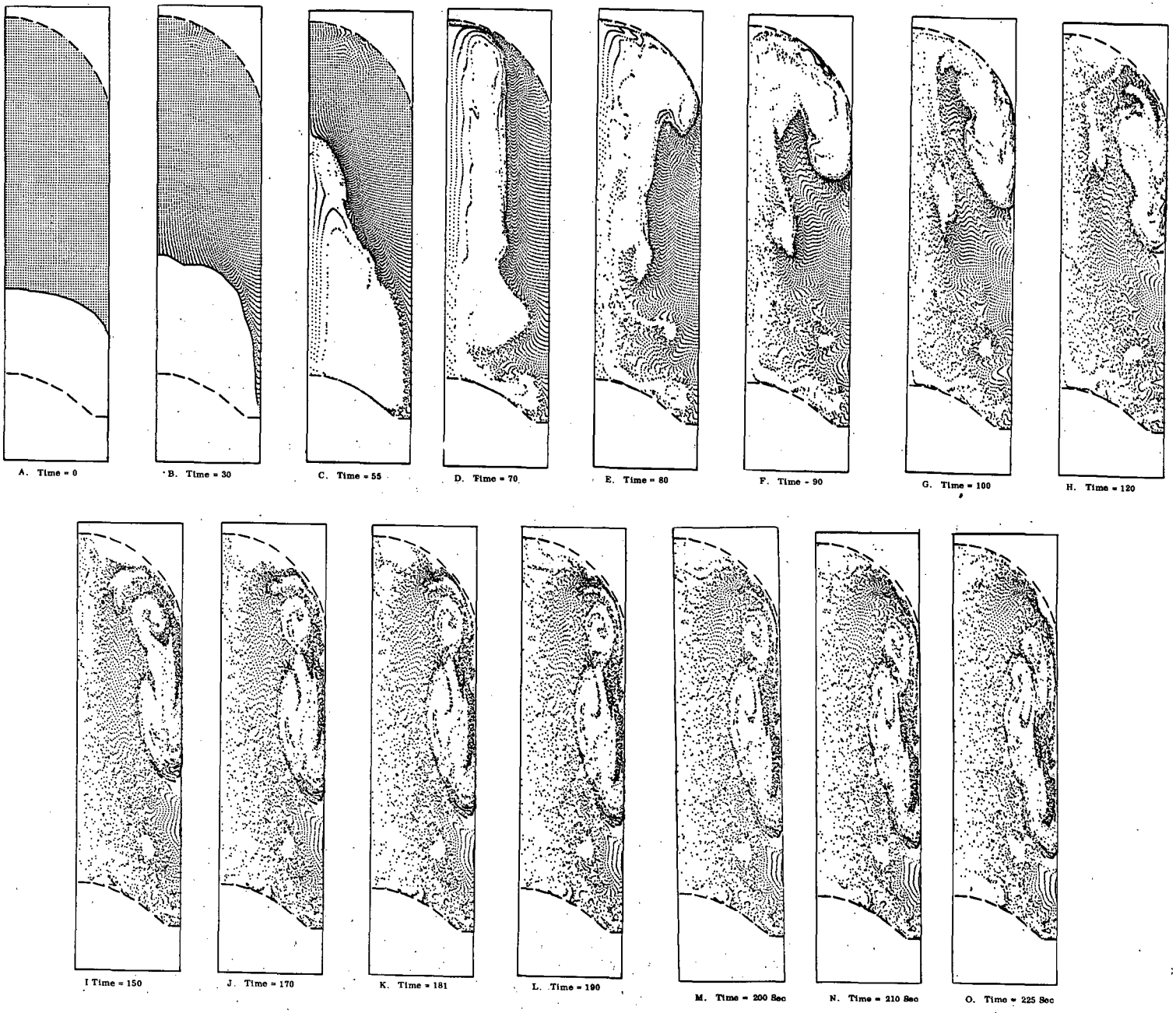

Figure 27. SC4020 Marker Particle Plots for Case 4

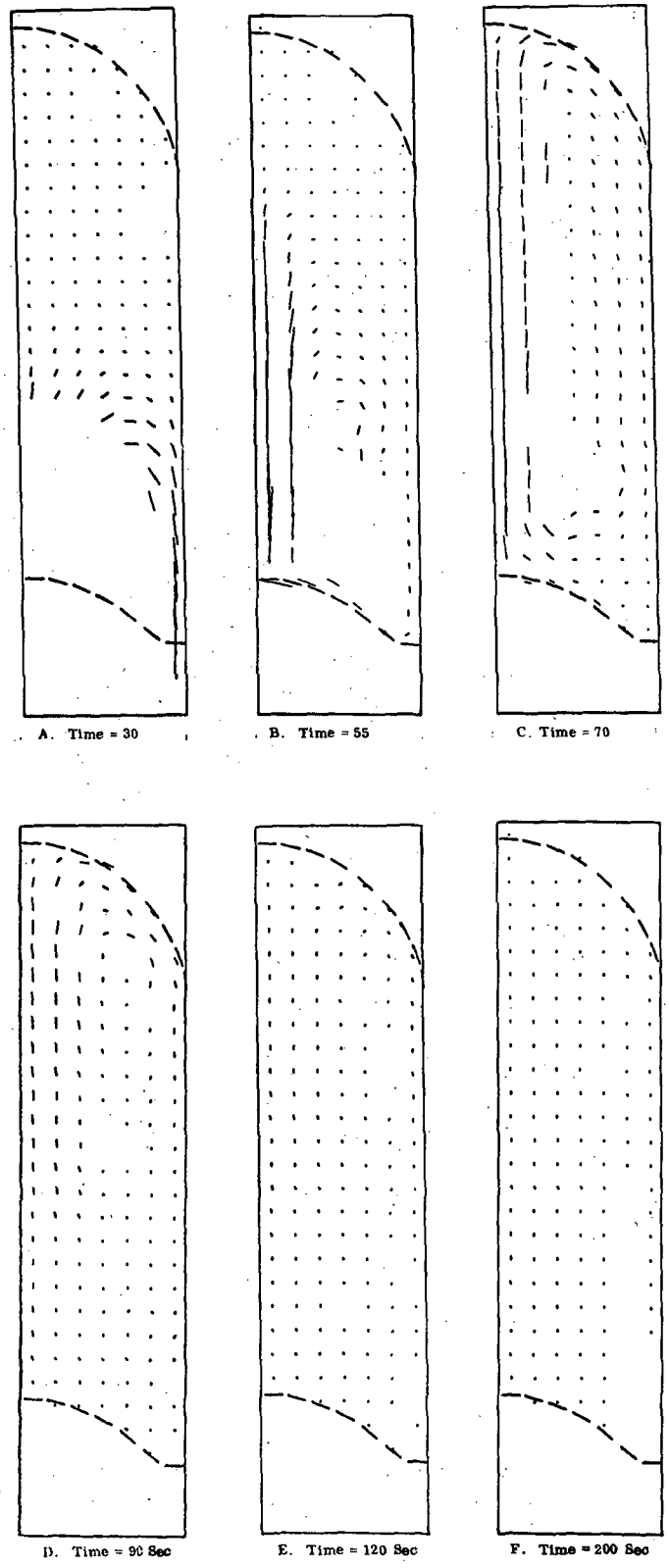

Figure 28. SC4020 Plots of Velocity Vector for Case 4

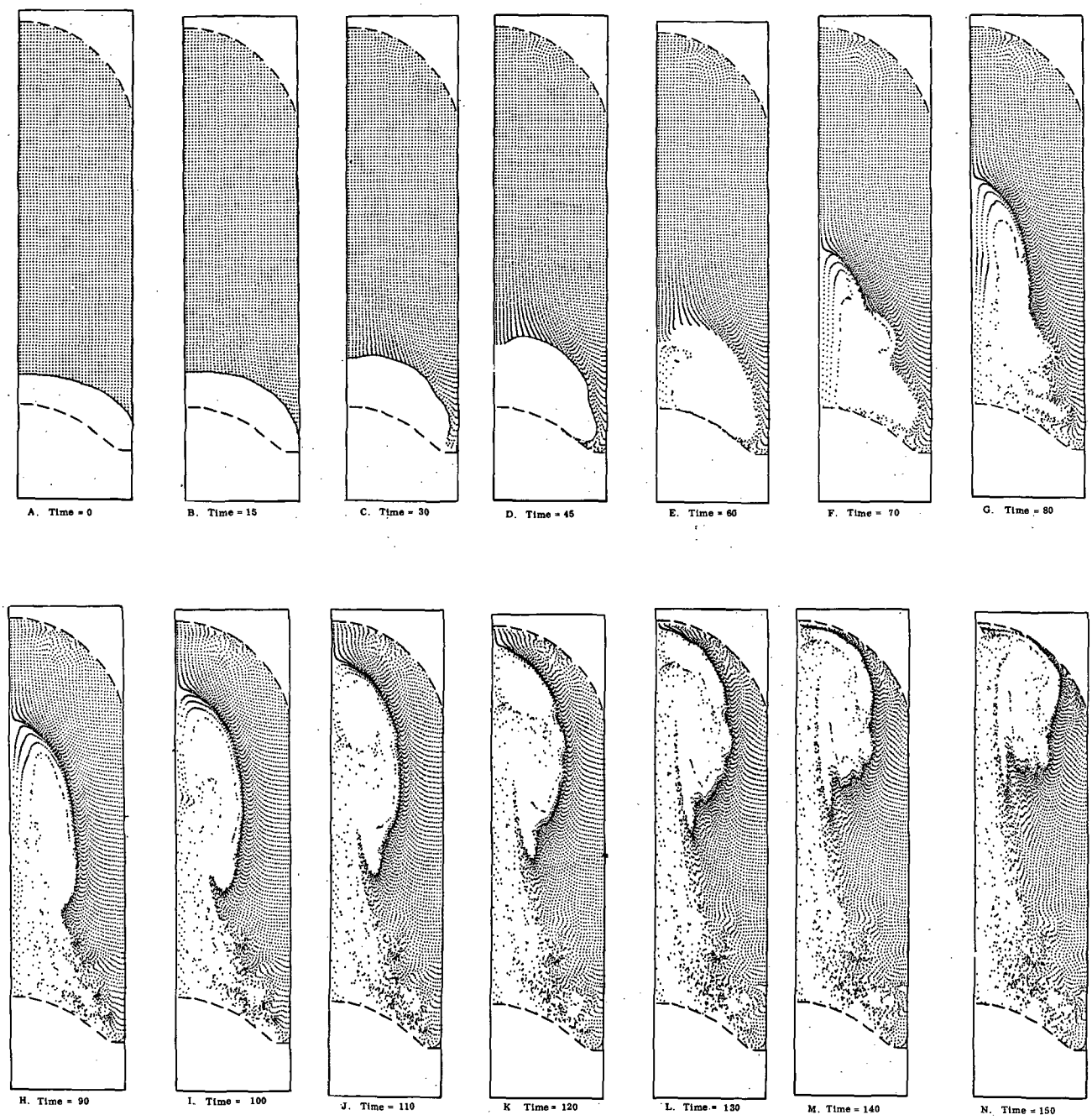

Figure 29. SC4020 Marker Particle Plots for Case 5

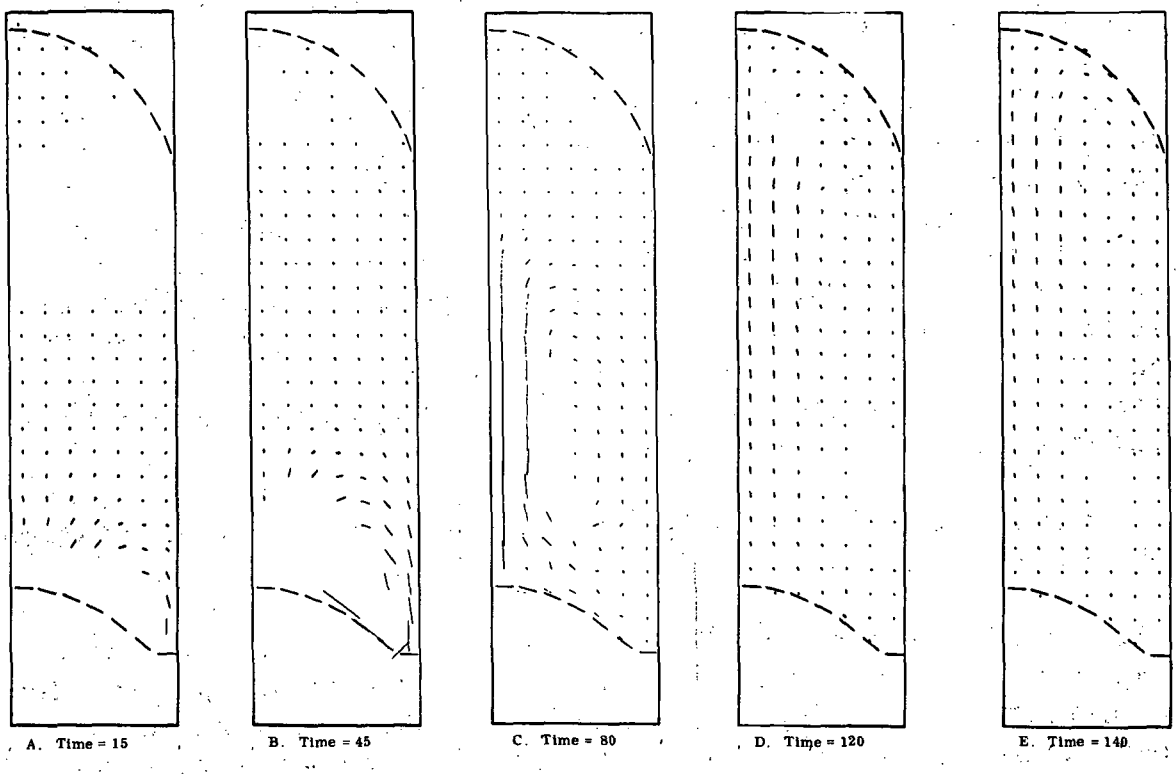

Figure 30. Velocity Vector Plots for Case 5

3.2.1 DISCUSSION OF RESULTS OF CASE 4.

- Initially the liquid moves down the wall of the container with a leading edge velocity that correlates with existing data (Reference 2). The fluid hits the truncated spherical bottom of the tank at 30.5 seconds with a leading edge velocity of 7.2 cm/sec.

- The liquid then travels along the bottom boundary as a thin film. The liquid is accelerated as it moves toward the center of the tank so that the velocity increases inversely with the tank radius. It is noted that turbulent viscosity does not yet have any affect at the lower right hand corner. This is because the turbulent viscosity (Section 2.1) is not considered in a corner which is surrounded only by surface cells. It is felt that the grid mesh should be finer at the lower right hand corner (and all corners) so that the turbulent viscosity can take affect. It is suspected that in this analytical run the fluid velocity across the bottom boundary is faster than would actually occur if turbulent viscosity were presented in the corner.

- The geyser forms at 45.3 seconds. Again turbulent effects are lacking because of the coarse grid mesh.

- The geyser forces its way through the fluid in the upper section of the tank as indicated in Figures 27C and 27D. The liquid continues to move down the walls of the tank and across the bottom boundary. While there is a lack of Marker particles next to the bottom tank wall in Figure 27D this region is considered to be full of fluid. This is noted in the velocity vectors in Figure 28C. It is noted that velocity vectors appear only in cells flagged either FUL or SUR.

- With increased time all the liquid initially in contact with the upper tank boundary is forced down the wall by the up coming geyser (Figures 27E and 27F). The amount of liquid collected is steadily increasing as indicated by Figure 31.

- The liquid becomes extremely turbulent in the upper region of the tank making it unclear if a region should actually be containing entrained vapor or not. This is the reason the collected liquid volume is not given after 100 seconds in Figure 31. By about 200 seconds (Figure 27M and 27N) the upper center region of the tank is clear. However, by 225 seconds (Figure 27O) the entire tank is considered by the program as full of fluid. This includes even the top of the tank. This is because of the coarse grid mesh which causes the entrained vapor to be lost in the liquid. This point is discussed in Section 3.2.3.

TOTAL LIQUID VOLUME = 2.47×10^7 cm^3

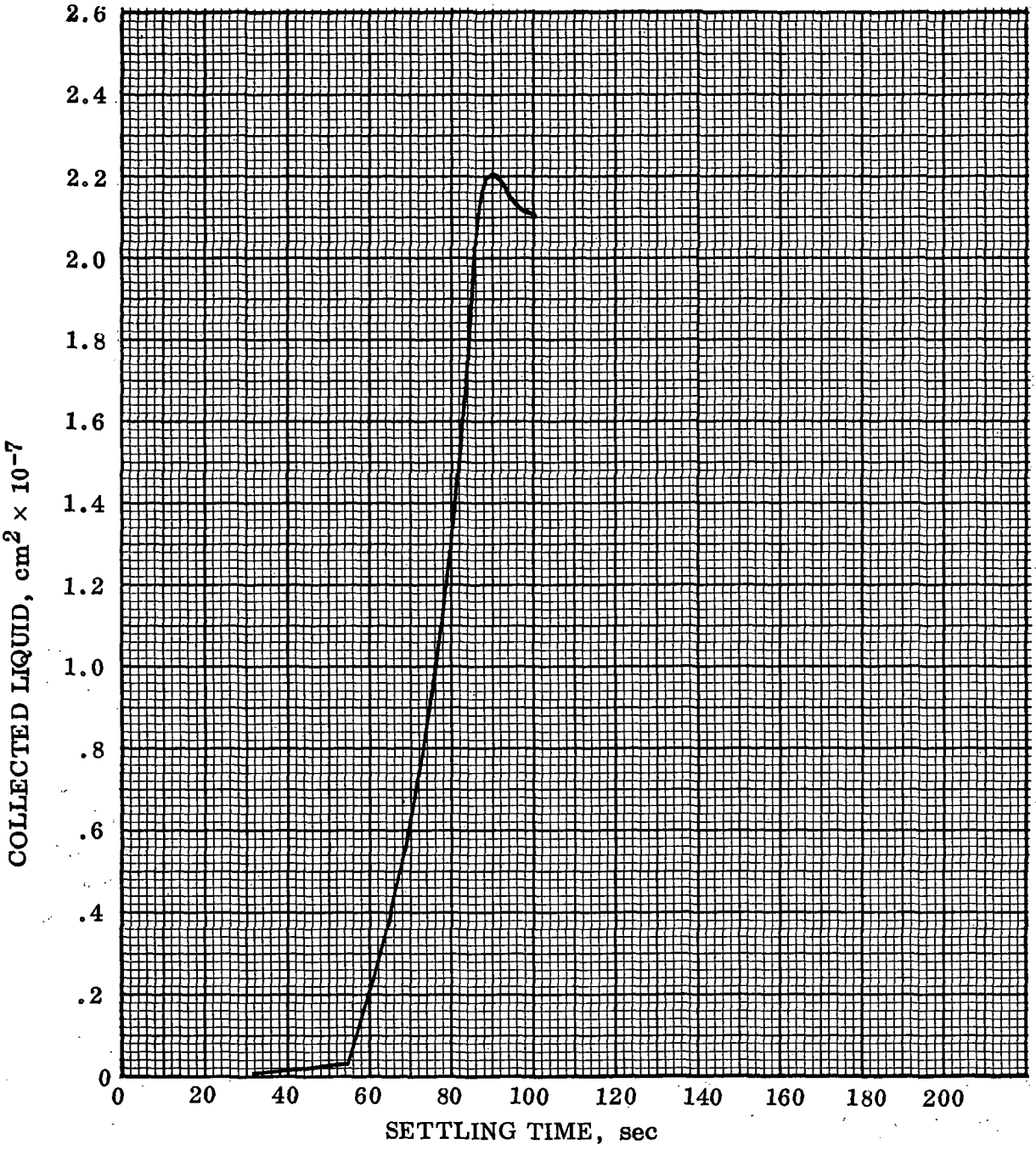

Figure 31. Collected Liquid Volume for Case 4

It is suggested that after approximately 100 seconds the loss in the calculation mesh of entrained bubbles begins to distort the results, since regions that should contain vapor are considered to be full of fluid. This distortion in the results becomes increasingly worse as more and more of the vapor gets lost in the fluid. By 200 seconds the tank is almost completely filled with fluid. At this time only the top most point is considered empty. However, there is still a sloshing motion of the fluid in the tank. In time (by about 225 seconds), this sloshing motion causes the entire tank region to be considered as full of fluid. It is noted that after 90 seconds the magnitude of the velocities of the fluid are continually decreasing with time. This can be seen by comparing Figures 28D, E, and F. The magnitude of the velocity vector is directly proportional to the length of the velocity vector lines in each plot. At 200 seconds, Figure 28E, the maximum velocity component in either direction (r or z) is less than 4 cm/sec.

In conclusion, after approximately 150 seconds the results for Case 3 have become so distorted by the lack of true empty cells that the results have only marginal significance.

3.2.2 DISCUSSION OF RESULTS FOR CASE 5.

- Initially the motion is the same as for Case 4. The liquid moves down the tank wall then accelerates across the bottom boundary. As the liquid converges at the center of the tank a geyser forms which impinges on the fluid in the upper region of the tank and then forces its way through the fluid.

- The collected volume (Figure 32) continues to increase as the gas in the tank appears to move up in a simple bubble (actually two bubbles since the SC4020 plots represent only half of a tank). It appears that as the bubble approaches the top of tank (until approximately 130 sec) there is not a significant amount of break up in the bubble. This implies no entrained vapor in the lower region of the tank.

- By 140 seconds, while it is still felt that the bubble is reasonably intact, the shape of the vapor region has been distorted so that actual resolution of the gaseous region is not possible because of the coarse grid mesh. This point is discussed in the following Section 3.2.3 and in Section 3.2.1.

3.2.3 GENERAL DISCUSSION OF RESULTS. While running Case 3 it was concluded that the grid mesh used was not fine enough to resolve the fluid motion. This was because the cell size was large relative to the liquid available. This resulted in nearly all the liquid appearing in cells flagged as SUR cells. While running Cases 4 and 5 the same type of problem developed; only in these cases the cell size was large

TOTAL LIQUID VOLUME FOR CASE 4 = 3.06×10^7 cm^3

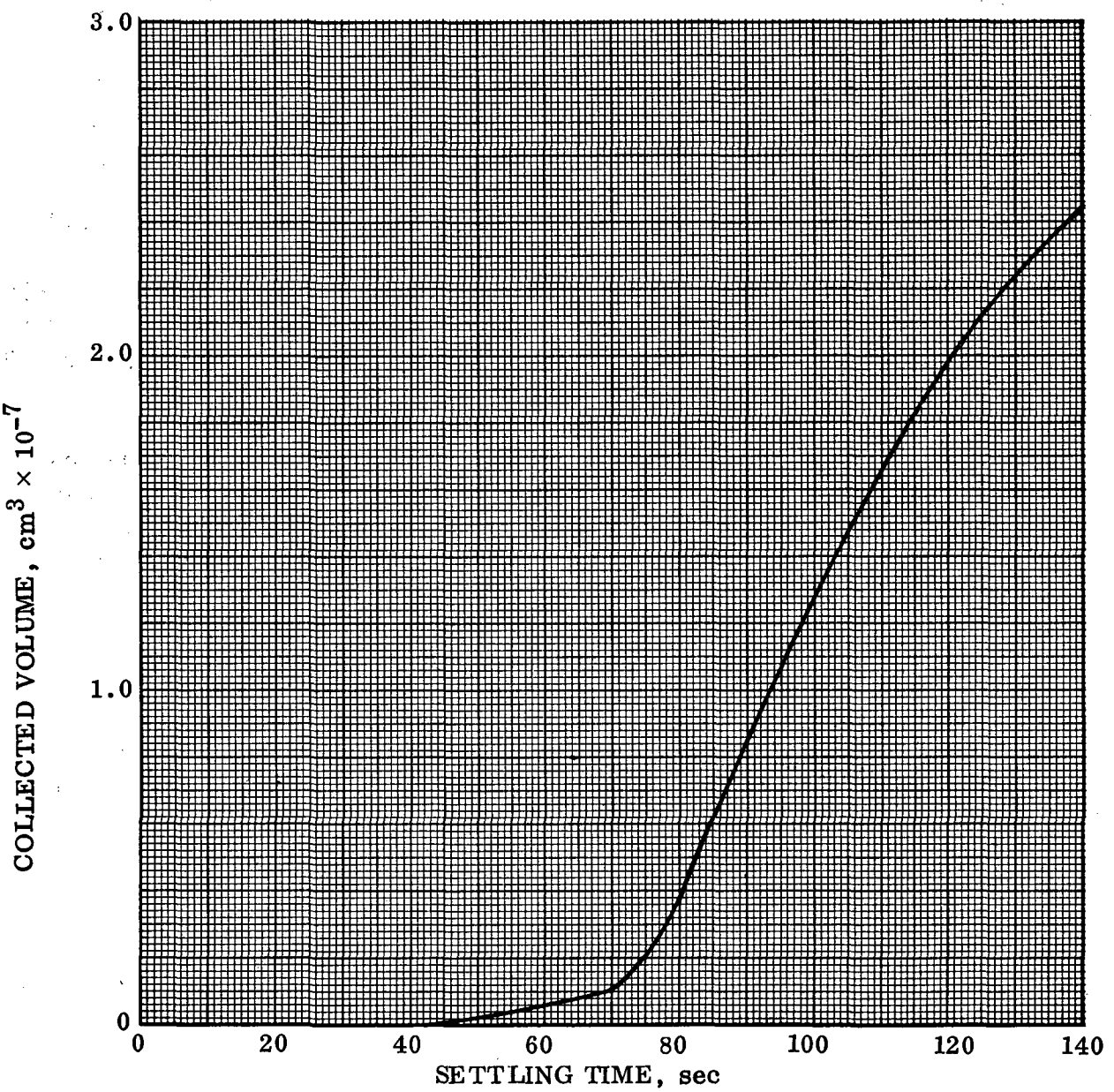

Figure 32. Collected Liquid Volume for Case 5

relative to the gas available. After a given length of time the condition developed where there was no empty (G = 4) cells. Figure 33 illustrates how a region containing a bubble which should be indicated as partly empty is indicated as a completely full section since no single cell is completely empty.

This is a serious problem since once the entire grid mesh contains no more G = 4 cells it is impossible to create G = 4 cells. This is because in SMAC a FUL cell must be a SUR cell before being empty (flagged G=4) and for a cell to be flagged SUR it must have an empty neighbor. In an attempt to remedy this problem, the condition was added that a FUL cell could be transformed directly into an EMP cell if the full cell lost all its marker particles. While this appears to give more meaningful results the abrupt change from FUL to EMP causes significant changes in the pressures which greatly increases the number of cycles required for convergence. Also, the fact remains that a region is at least temporarily flagged as full when it is at least partially empty.

It is concluded that not only should the cell size be small compared to the fluid available but should also be small compared with the gas available. This was not

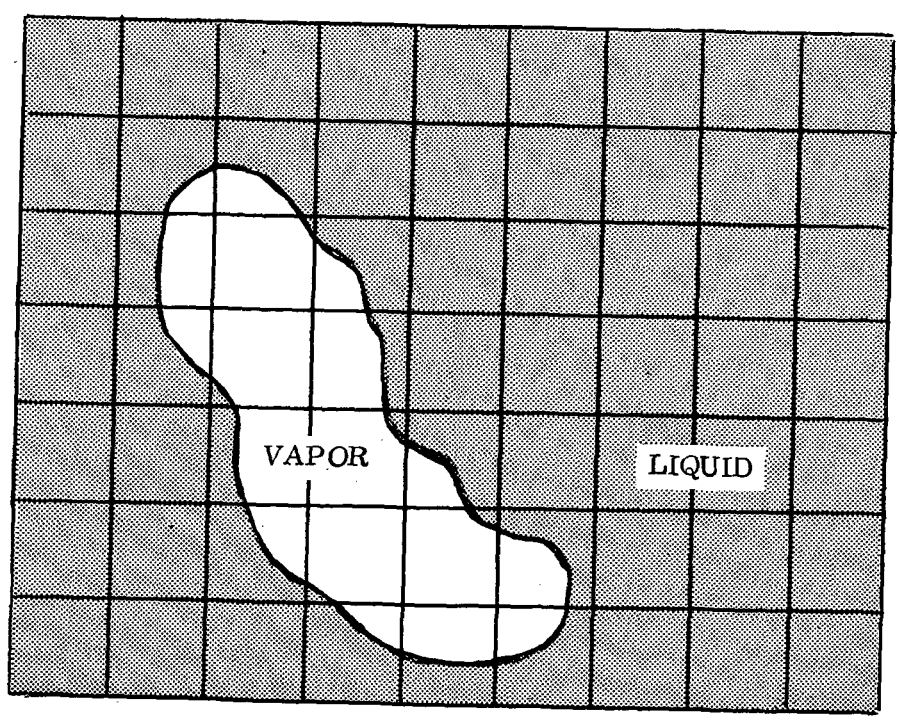

Figure 33. Vapor Bubble Located on a Coarse Grid Mesh

true for Case 4 which initially had only 13 cells flagged as empty (G = 4) and 7 of these G = 4 cells were along the arbitrary boundary which is not even a whole cell.

Since the problems encountered in Case 2 and Cases 3 and 4 result from the grid mesh being too coarse it is concluded that the complex problem of liquid reorientation in a tank requires a finer mesh than what has been used during this contract. This problem will be even more severe for simulations with internal baffles which are characterized by extreme turbulence. It is therefore suggested that HOPI be modified to reduce the computer core required to run a problem and that every iteration loop be optimized. The core required for problems 1 through 5 was approximately 131,000 for the initial setup (with ARBND) and 123,000 for successive runs (without ARBND and VOLUME). It is felt that by using "overlay" the core could be reduced to below 100,000. This would not only reduce computer cost but would also make available the additional core required when a finer grid mesh is needed.

4.0 CONCLUSIONS AND RECOMMENDATIONS

During this contract a computer program called HOPI was developed. This program uses the Simplified Marker and Cell, SMAC, numerical technique. HOPI has shown that it can analytically determine the fluid motion in a cryogen storage tank under a continuous settling load. The equations programmed in HOPI are applicable to Newtonian incompressible fluid. HOPI can be used with curved boundaries. While the grid dimension can differ in the radial, DR, and axial, DZ, direction; HOPI can presently handle only a constant-size grid mesh. Experience has indicated that this is a serious limitation since a finer grid mesh is usually needed at corners and along the boundaries than is needed in the middle region of the tank. It would be extremely inefficient to use the smallest needed cell throughout the grid mesh. Currently HOPI and the related subroutines are loaded into the computer core at the same time. This causes an unnecessarily high demand for core. In fact, the grid size used for a typical problem loads the core to near capacity. It is estimated that if the radial and grid dimension were both reduced by half, thereby multiplying by a factor of four the grid size, the core of the computer would be exceeded. However, experience indicated that a reduction of the grid dimensions by at least half is needed to accurately resolve the fluid motion under a number of conditions. This is especially true if there is less than 25% liquid or gas or if the liquid becomes extremely turbulent.

HOPI has a surface pressure interpolation scheme which is required to avoid unrealistic surface breakup. This scheme sets the pressure in the middle of a surface cell so that the pressure at the actual surface of the liquid is correct.

HOPI uses the equation

$$\nu_{turb} = TURB \times \ell^2 \max\left(\left| \frac{\partial v}{\partial r} \right|, \left| \frac{\partial u}{\partial z} \right| \right)$$

to simulate a turbulent viscosity, ν_{turb}, where

$$\ell = \begin{cases} DR \text{ if } \left|\frac{\partial v}{\partial r}\right| > \left|\frac{\partial u}{\partial z}\right| \\ \\ DZ \text{ if } \left|\frac{\partial u}{\partial z}\right| > \left|\frac{\partial v}{\partial r}\right| \end{cases}$$

and

v is the radial component of velocity

u is the axial component of velocity

TURB is an empirical input quality. It has been found that the use of a proper value of TURB does aid in correlating the analytical results with the test results. Experience has also indicated that the determination of the "collected liquid volume" is best determined from an examination of the SC4020 Marker particle plots. Lastly, the subroutine written to determine "collected liquid volume" has not proven very useful, especially where turbulence causes vapor entrainment in the liquid.

For the future work, the following changes in HOPI are recommended.

1. The subscripting should be changed from a double to a single throughout the code. This will reduce the computer running time for a given problem.

2. Use overlay to reduce the core needed for a given size problem.

3. Delete subroutine VOLUME. Because of its limited usefulness, it appears that it can be deleted. Furthermore this will reduce the core required for a given problem.

4. For a half tank simulation,set-up the case with finer grid than the 288 cells used to define the tank during this contract.

5. Introduce a variable grid mesh. This will allow more efficient use of the computer by using smaller grid sizes where needed but allowing larger size grids where possible.

6. Develop a surface pressure interpolation scheme which can be used even after the geyser impinges on the liquid in the upper region of the tank.

APPENDIX A

SELECTION CRITERIA FOR THE MINIMUM, MEAN AND MAXIMUM COLLECTED LIQUID HEIGHT

The definition of the "collected liquid" height is the height below which liquid and no vapor exist. As can be seen in the Marker particle plots this height is often difficult to define. This is because a cell is considered full once it contains a single marker particle. Therefore, the fact that the region looks nearly free of particles or at least the particles are rarified when compared to other regions does not in itself indicate that vapor exists in this region. Secondly, the coarse grid mesh, while needed to avoid excessive time steps during computation, results in inaccuracies in the fluid motion. When the velocity vectors of adjacent cells deviate by more than 90° (see Figure 20C) the result is an unrealistic dip in the fluid as indicated in Figure 19H.

A basic criteria used to estimate the collected liquid height is presented in the following paragraphs. It is used only as a guide and is not an absolute criteria.

Up to 1.416 seconds (Figure 19F) there is only one height. Initially this height was computed using the assumption that the height equalled the actual minimum level of the particles. Then as the dip in the surface became more pronounced as in Figure 19F, the dip portion was considered as actually containing particles.

Starting with Figure 19G more than one height is indicated because of ambiguity in what is the true "collected liquid" height. Starting with Figure 19H three heights are usually indicated. These heights were estimated as follows.

Minimum Height. Assumes that the dominant lowest dip in the surface is actually filled with particles to the point where there is an abrupt change in direction in the particles outlining the surface of the geyser. In Figure 19H this point is noted by (1).

Mean Height. Assumes that particles actually fill up the void to the point where the particles nearest the bottom yet in the fluid coming down the wall start to move toward the center of the tank instead of directly toward the bottom. In Figure 19H this point is noted by (2). Or, as is the case in Figure 19L, the mean height is estimated as existing at the highest point of the fluid initially from the side fluid and which was not part of the geyser fluid.

Maximum Height. There are two methods for estimating the maximum height. One assumes that the "collected liquid" is to the point where the particles in the fluid coming down the wall first start to move toward the center of the tank instead of directly down. In Figure 19H this point is noted by (3). The other assumes that the height exists where the geyser has collapsed and flowed toward the liquid on the side of the tank and is in contact with the fluid coming down the side of the tank wall. Contact exists when particles of the geyser side and particles in the wall side occupy part of the same cell. This criteria is illustrated in Figure 19J.

APPENDIX B

NOMENCLATURE

A	area
Bo	Bond number, gR^2/β
D	velocity divergence = $(1/r^{\alpha})\ (\partial r^{\alpha} u/\partial r) + (\partial v/\partial z)$
DR	grid dimension in the radial direction
DZ	grid dimension in the axial direction
G	cell flag
g_r	radial acceleration
g_z	axial acceleration
i	radial spatial coordinate index
j	axial spatial coordinate index
m	boundary slope
n	time index number of cycles
$\hat{n}$	unit normal defining a boundary segment
P	pressure
P_{ij}	pressure of cell ij
r	radial coordinate
R	tank radius
RELAX	relaxation parameter
S	Poisson source term
TURB	empirical factor for turbulence
t	time
u	radial component of velocity
$\tilde{u}$	radial storage variable, radial component of the tilde velocity
v	axial component of velocity
$\tilde{v}$	axial storage variable, axial component of the tilde velocity
V	velocity

V_p	liquid velocity at midpoint of boundary segment computed with the MAC area weighing interpolation scheme
$\vec{X}_n$	position of midpoint of a boundary segment
$\vec{X}_p$	position of particle
z	axial coordinate
α	geometric parameter, $\alpha = 1.0$ in cylindrical coordinates and equals 0.0 in plane (cartesian) coordinates
β	specific surface tension
δr	incremental step in the r direction
δz	incremental step in the z direction
Δt	time step
Δr	radial mesh width
Δz	axial mesh width
ϵ	boundary sensing parameter
λ	minimum mesh dimension, minimum of DR or DZ
υ	kinematic viscosity
ρ	density
ϕ	true pressure normalized to unit density
σ	$\Delta t/\rho$
ψ	arbitrary pressure normalized to unit density (pseudopressure)
ω	vorticity
∇	gradient operator

Superscripts

k	iteration index
n	counts time cycles

Subscripts

i	position in the finite-difference mesh
j	position in the finite-difference mesh
p	located at midpoint of boundary segment

REFERENCES

1. Bowman, T. E., "Cryogenic Liquid Experiments in Orbit, Volume I: Liquid Settling and Interface Dynamics," NASA CR-651, 1966.

2. Salzman, J. A. and W. J. Masica, "Experimental Investigation of Liquid-Propellant Reorientation," NASA TN D-3789, 1967.

3. Hollister, M. P., H. M. Satterlee and H. Cohan, "A Study of Propellant Behavior During Periods of Varying Accelerations," NASA CR-92084, 1967.

4. Blackmon, J. B., "Propellant Settling," Douglas Missile and Space Systems Division Report DAC-62263, 1968.

5. Labus, T. L. and W. J. Masica, "Liquid Reorientation in Spheres by Means of Low-G Accelerations," NASA TM X-1659, 1968.

6. Perko, L. M., "Large Amplitude Motions of a Liquid-Vapor Interface in an Accelerating Container," J. Fluid Mech., Vol. 35, 1969, pp 77-96.

7. Bowman, T. E., "Sheet of Liquid Flowing Down a Wall," The Physics of Fluids, Volume 14, Number 7, July 1971, pp 1578-1579.

8. Amsden, Anthony A. and Harlow, Francis H., "The SMAC Method: A Numerical Technique for Calculating Incompressible Fluid Flows," Los Alamos Scientific Laboratory Report No. LA-4370, Feb. 17, 1970.

9. Viecelli, James A., "A Computing Method for Incompressible Flows Bounded by Moving Walls," Lawrence Radiation Laboratory Report UCRL-72815, September 1970.

10. Betts, W. S., "A SMAC Computer Code With Arbitrary Boundaries: HOPI, Program P5623," Convair Aerospace Report 632-1-85, 19 April 1972.

11. Hirt, C. W., "Heuristic Stability Theory for Finite Difference Equations," J. Computational Physics, Volume 2, 1968, pp 339.

12. Coney, T. A., "Surface Tension Viscosity and Density Measurements of Two Fluorocarbon Solvents, FC-43 and FC-78," NASA Technical Memorandum TM X-1862, August 1969.

DISTRIBUTION LIST - NAS3-14361

Name	No. of Copies
NASA Scientific & Technical Information Facility Box 33 College Park, Maryland 20740 Attn: NASA Representative	2
National Technical Information Service Springfield, Virginia 22151	40
NASA-Lewis Research Center 21000 Brookpark Road Cleveland, Ohio 44135 Attn: Wm. J. Masica, Mail Stop 500-318	25
Astronautic/Propulsion Mail Stop 1662 Martin Denver Division Denver, Colorado 80201	1
Mr. K. R. Burton 647 Noble Road Marysville, California 95901	1
Factory Mutual Research Corporation 1151 Boston-Providence Turnpike Norwood, Massachusetts 02062 Attn: Dr. John deRis	1
Florida Institute of Technology Space Technology Dept. Melbourne, Florida 32901 Attn: Dr. T. E. Bowman	1
General Applied Science Labs, Inc. Merrick and Stewart Avenues Westburn, L.I., New York 11590 Attn: Dr. Raymond Edelman	1
University of California Los Alamos Scientific Laboratory P.O. Box 1663 Los Alamos, New Mexico 87544 Attn: Dr. Francis H. Harlow	1
John Carroll University Dept. of Physics University Heights, Ohio 44118 Attn: Dr. E. F. Carome	1
John Carroll University Dept. of Physics University Heights, Ohio 44118 Attn: Dr. K. Fritsch	1

Name	No. of Copies
Lockheed Missiles and Space Company Spacecraft Thermodynamics Dept. Sunnyvale, California 94008 Attn: Dr. H. M. Satterlee	1
Lockheed Missiles and Space Company Spacecraft Thermodynamics Dept. Sunnyvale, California 94008 Attn: Dr. G. D. Bizzell	1
Manned Spacecraft Center 2101 Webster-Seabrook Road Mail Stop E.P. 2 Houston, Texas 77058 Attn: Z. D. Kirkland	1
Marshall Space Flight Center Huntsville, Alabama 35812 Attn: L. Hastings/S&E-ASTN-PFA	1
Marshall Space Flight Center Huntsville, Alabama 35812 Attn: A. L. Worlund/S&E-ASTN-PF	1
McDonnell-Douglas Astronautics Co. 5301 Bolsa Ave. Huntington Beach, California 92647 Attn: J. B. Blackmon	1
McDonnell-Douglas Astronautics Co. 5301 Bolsa Ave. Huntington Beach, California 92647 Attn: Dr. R. A. Madsen	1
NASA-John F. Kennedy Space Center Kennedy Space Center, Florida 32899 Attn: W. G. Boggs/DD-SED-4	1
North American Aviation, Inc. Space and Information Systems Div. 12214 Lakewood Blvd. Downey, California 90241 Attn: Don Gluck	1
Office National D'Etudes Et De Recherches Aerospatiales 29, Avenue de la Division LeClerc 92 Chatillon France Par Michel Delattre	1
Office National D'Etudes Et De Recherches Aerospatiales 29, Avenue de la Division LeClerc 92 Chatillon France Par Jean Maulard	1

Name	No. of Copies
RCA/AED P.O. Box 800 Princeton, N.J. Attn: Mr. Daniel Balzer	1
Southwest Research Institute Dept. of Mechanical Sciences P.O. Drawer 28510 San Antionio, Texas 78284 Attn: H. Norman Abramson	1
Tufts University Mechanical Engineering Dept. Medford, Massachusetts 02155 Attn: Dr. Lloyd Trefethen	1
Lawrence Berkeley Laboratory Berkeley, California 94720 Room 50-A-1140 Berkeley, California 94720 Attn: Dr. Paul Concus	1
University of Kentucky Lexington, Kentucy 40506 College of Engineering Attn: Dr. John H. Lienhard	1
University of Michigan Ann Arbor, Michigan 48107 Attn: Dr. H. Merte, Jr.	1
University of Tennessee Knoxville, Tennessee 37916 Dept. of Mechanical and Aerospace Engineering Attn: Franklin T. Dodge	1
University of California Lawrence Radiation Laboratory P.O. Box 808 Livermore, California Attn: Mr. J. A. Viecelli	1

GENERAL DYNAMICS

Convair Aerospace Division